Impact of climate change on the ecology of the Kyambangunguru crater marsh in southwestern Tanzania during the Late Holocene

Impact of climate change on the ecology of the Kyambangunguru Crater Marsh in southwestern Tanzania during the Late Holocene

Sarah Coffinet[a1], Arnaud Huguet[a], Laurent Bergonzini[b], Nikolai Pedentchouk[c], David Williamson[d], Christelle Anquetil[a], Mariusz Gałka[e], Piotr Kołaczek[e], Monika Karpińska-Kołaczek[e, f, g], Amos Majule[h], Fatima Laggoun-Défarge[i], Thomas Wagner[j], Sylvie Derenne[a]

[a]*Sorbonne Université, CNRS, EPHE, PSL, UMR METIS, Campus Pierre et Marie Curie, 4 place Jussieu, 75252 Paris cedex 05, France*

[b]*Université Paris Saclay, UPS Univ Paris 11, CNRS, UMR GEOPS, rue du belvédère, Bât 504, 91405 Orsay cedex, France*

[c]*School of Environmental Sciences, University of East Anglia, Norwich Research Park, Norwich, NR4 7TJ, United Kingdom*

[d]*Sorbonne Université, Institut de Recherche pour le Développement, MNHN, CNRS, UMR LOCEAN, Centre IRD France Nord, F-93143, Bondy cedex, France*

[e]*Department of Biogeography and Paleoecology, Faculty of Geographical and Geological Sciences, Adam Mickiewicz University in Poznań, Krygowskiego 10, 61-680 Poznań, Poland*

[f]*Laboratory of Wetland Ecology and Monitoring, Faculty of Geographical and Geological Sciences, Adam Mickiewicz University in Poznań, Krygowskiego 10, 61-680 Poznań, Poland*

[g]*Centre for the Study of Demographic and Economic Structures in Preindustrial Central and Eastern Europe, University of Bialystok, Plac Uniwersytecki 1, 15-420 Białystok, Poland*

[h]*Institute of Resource Assessment, University of Dar Es Salaam, P.O. Box 35097, Dar Es Salaam, Tanzania*

[i]*Université d'Orléans, CNRS, BRGM, UMR ISTO, 1A rue de la Férollerie 45071 Orléans, France*

[j]*Heriot-Watt University, Lyell Centre for Earth and Marine Science and Technology, School of Energy, Geoscience, Infrastructure and Society (EGIS), Edinburgh, EH14 4AS, United Kingdom*

Corresponding author email address: scoffinet@marum.de ; +49 421 218 65740

[1] Present address: Organic Geochemistry Group, MARUM - Center for Marine Environmental Sciences & Department of Geosciences, University of Bremen, Leobener St. 8., Bremen, Germany

Abstract

Instrumental records of temperature and hydrological regimes in East Africa evidence frequent droughts with dramatic effects on population and ecosystems. Sources of these climatic variations remain largely unconstrained, partly because of a paucity of Late Holocene records. Here, we present a multi-proxy analysis of a 4-m continuous sediment core collected in the Kyambangunguru crater marsh, in southwest Tanzania, covering the last 4000 yrs (cal. BP). We used microscopic (macro-remains, microfossils, palynofacies, pollen), elemental (carbon, nitrogen contents), molecular (br GDGTs, *n*-alkanes) and compound-specific isotopic (δ^2H *n*-alkanes) investigations to reconstruct the environmental history of the marsh. The multi proxy record reveals that, 2500 years ago, the marsh underwent a major ecological transition from a lake to a peatland. Temperature and hydrological reconstructions evidence warmer and drier conditions between 2200 and 860 cal. BP, which probably triggered the establishment of a perennial peatland. This study is one of the first combined temperature and precipitation record of Late Holocene in the region and highlights changes in the spatial distribution of the East African climate regimes. Several cold periods are observed, between 3300 and 2000 cal. BP and since 630 cal. BP, the latter corresponding to the Little Ice Age. Moreover, wetter conditions are reported during the Medieval Climate Anomaly in contrast to other north-eastern African records suggesting that Tanzania is located at the transition between two hydro-climatic zones (north-eastern versus southern Africa) and has experienced variable contributions of these two zones over the last millennium.

Keywords

Holocene, Paleoclimatology, Paleolimnology, East Africa, Continental biomarkers, Organic geochemistry, Stable isotopes, Palynology.

1. Introduction

Tropical highlands are major sources of food and freshwater for more than 35 tropical countries (Williamson, 2014). The climate dynamics and variability of these topographically complex environments, however, remain poorly studied. While it has been shown that the Quaternary climatic trends in East Africa were primarily controlled by orbital forcing (e.g. Garcin et al., 2006; Tierney et al., 2008), the shorter scale climate dynamics of this region is largely unconstrained. Notably, mid- to late Holocene records of many East African lakes (e.g. Gasse, 2000; Wanner et al., 2011) suggest rapid and frequent, high amplitude, climatic fluctuations at the centennial scale. These fluctuations and their consequences are not well understood due to a general lack of highly resolved records (Nicholson et al., 2013). Furthermore, the timing and intensity of these events are not always synchronous from site to site (Tierney et al., 2011, 2013). Here, we present detailed records of climate and ecosystem changes from a sequence of sediments covering the late Holocene (the last 4000 years) in the Kyambangunguru marsh. This marsh is located in the Rungwe Volcanic Province (RVP; southwest Tanzania), a highland representing one of the four major food crop producing regions in the country (Majule, 2010).

Marshes and peatlands have a great potential for quantitative high-resolution palaeoclimatic records (Amesbury et al., 2012; Blackford, 2000) notably in the tropics (e.g. Bonnefille et al., 1990; Bourdon et al., 2000; Page et al., 2011; Rucina et al., 2010; Swindles et al., 2018). However, they are highly dynamic ecosystems where the vegetation cover and the hydrology functioning can be totally modified at a centennial scale (Loisel and Yu, 2013). This may complicate the interpretation of climatic proxies, notably those based on biological markers as their fluctuations may be related to ecological, local change rather than regional climatic change. A major challenge in using marsh/peat records as climatic archives is thus to disentangle biological signals linked to dynamic changes of the peatland ecosystem itself from those that are driven by local to regional environmental change (Chambers et al., 2012; Morris et al., 2015). The focus of this study is to investigate the internal, ecological changes within the marsh in the context of regional climatic variations. We aim to retrieve detailed (quantitative) air temperature and (qualitative) hydrological condition records of the late Holocene from the southernmost part of East Africa to test whether rapid and high amplitude climatic events (e.g. Russell and Johnson, 2005; Wanner

et al., 2011) were recorded in this area in comparison to other East African records. Additionally, the multi-proxy approach, combining microscopic observations and geochemical characterization, intends to determine potential feedbacks of these rapid climatic events in the tropical highland wetlands as well as potential human impact in the region.

Analysis of pollen, non-pollen palynomorphs (NPPs), macro-remains, palynofacies and bulk elemental (C and N content) determination was conducted to characterize the ecological states of the wetland, complemented by biomarker-based proxies to determine past variations in air temperature and hydrology. Branched glycerol dialkyl glycerol tetraethers (br GDGTs) and compound specific long chain *n*-alkane hydrogen isotopic composition (δ^2H_{wax}) were used for mean annual air temperature and hydrological conditions reconstruction, respectively. Br GDGTs are membrane lipids produced by unknown bacteria (Sinninghe Damsté et al., 2000) whose relative abundances in environmental samples have been shown to correlate with temperature and pH (Weijers et al., 2006, 2009). This enabled the reconstruction of past pH and air temperatures from the br GDGT distribution in sediments, peats and soils (Nichols et al., 2014; Peterse et al., 2011; Weijers et al., 2007a). Long chain *n*-alkanes are constituents of the epicuticular wax layer of leaves (Eglinton and Hamilton, 1967). It has been shown that their hydrogen isotopic composition (δ^2H_{wax}) reflects the hydrogen isotopic composition of the water taken up by the plants (e.g. Estep and Hoering, 1980; Sauer et al., 2001; Sessions et al., 1999). Accordingly, they can be used to reconstruct variations in local palaeohydrology as shown in several lacustrine sedimentary archives from the Quaternary and the Holocene in East Africa (e.g. Loomis et al., 2015; Powers et al., 2005; Tierney et al., 2008; Verschuren et al., 2000). The combined use of these two proxies allows distinguishing the temperature from the hydrological signal which has been a major limitation in lake-based East African climatic reconstructions (Verschuren, 2003). Moreover, in settings with high sedimentation rates like marshes, they can offer highly detailed and independent reconstruction of the temperature and the hydrological conditions.

2. Regional setting: the Rungwe Volcanic Province and the Kyambangunguru marsh

The Rungwe Volcanic Province (RVP; SW Tanzania; Fig. 1A), is a large volcanic mountain region (1500 km²) located at the triple junction of the Malawi Rift, Rukwa/Tanganyika Rift and the Usanga Basin in the southern part of the East African Rift System (Fontijn et al., 2010, 2012). The RVP is delimited by the Poroto Mountains in the north, Lake Malawi in the south and the Livingstone escarpment in the west (Fig. 1B). The area is known to be seismically active with volcanic eruptions occurring from the late Miocene (9.2 Ma) to the 19th century, with hot spring activity still found today (Branchu et al., 2005). The region contains three major stratovolcanoes: the Ngozi, Kyejo and Rungwe (Fontijn et al., 2010, 2012). South of these high-altitude sites and north of Lake Malawi lies the Karonga plain. Several monogenic maar-type craters were created during late Pleistocene phreatomagmatic explosions along the Mbaka fault system and are now filled by closed lake hydro-systems (Fontijn et al., 2012; Fig. 1B). The region belongs to the humid equatorial zone of Africa, mainly determined by the migration of the Intertropical Convergence Zone (ITCZ), a key atmospheric feature of tropical atmospheric circulation with low-pressure air masses accompanied by high precipitation. The ITCZ reaches its southernmost position (centred at ca. 15°S, Fig. 1A) in January, resulting in seasonal fluctuations between hot humid conditions from November to May and relatively colder and dry conditions from June to October (Fig. 1C). The RVP is among the most humid regions of Tanzania along with the coastal zone (Basalirwa et al., 1999). It is characterized by a different rainfall distribution with persisting rainfall in April-May. Nivet et al. (2018) showed that the Indian tropical Ocean and the Austral Ocean are the main sources of moisture in the area, with only a minor influence of the Congo Air Mass. Thus, the currently observed variability of the regional rainfall is likely highly impacted by the Indian Ocean Dipole, through Sea Surface Temperature anomalies. Over the last century, climatic trends from the RVP point towards drier conditions associated with a shorter rain season (Williamson et al., 2014) and a continuous increase in temperature (≈ 1°C for the last 100 yr.; Branchu et al., 2005). Typical vegetation of the region includes Zambezian Miombo-type woodland at low altitude and Afromontane vegetation at higher altitude (Garcin et al., 2006, Williamson et al., 2014). In many locations, the woodland has been replaced by diverse crops (banana, rice, cocoa, tea, coffee, maize;

136 Coffinet et al., 2017; Williamson et al., 2014). The RVP is today one of the main agricultural resources
137 of Tanzania (Majule, 2010).
138 The Kyambangunguru marsh (9°22' S - 33°47' E, 660 m a.s.l.) is located in one of the numerous maar
139 craters of the RVP, between the Mbaka River and the Mbaka fault. These maar craters are essential
140 water and biodiversity resources for the region. At Kyambangunguru, no human activity has been
141 recorded nor is known within the crater (no land or water use). Human settlement expands in the plains
142 surrounding the volcano (mainly family-scale farming) but not on its slopes. The inner marsh covers
143 about 0.04 km^2 and its catchment area – limited to the crater slopes elevated ca. 100 m above the water
144 table – is relatively small (0.20 km^2; Delalande et al., 2008a, Fig. 1D). According to the Lwifwa Masoko
145 station of the University of Dar es Salaam located at Lake Masoko, 7.5 km to the south east, mean
146 precipitation (P) is up to 2099 $mm.yr^{-1}$, with April being the most humid month (470 mm in average)
147 and September the driest one (8 mm in average; Nivet et al., 2018). Air temperature fluctuates around
148 22 °C throughout the year; July is the coldest month (19 °C on average) and November the warmest (25
149 °C on average). The crater depression is filled with peat like deposits overgrown by marsh-type
150 vegetation and the water level (H) varies around 70 cm of amplitude over the year (Fig. 1C). At the end
151 of the rainy season, the marsh resembles a shallow lake with floating vegetation mats and patches of
152 free water surface (Fig. 1E) while the water table considerably decreases during the dry season (Fig.
153 1C). On a monthly scale, water level fluctuations (ΔH) correlate with the rainfall (P): $\Delta H = 1.03\ P - 18$
154 (in cm; n = 12; r = 0.97). During the humid season, the marsh water is warm (around 25 °C), low
155 mineralized and slightly acidic (pH around 5.8). On the contrary, during the dry periods, it is
156 characterized by higher mineral concentration as well as pH increase up to around 6.4, because of water
157 evaporation at the surface (Delalande, 2008; Delalande et al., 2008a). The water residence time in the
158 marsh is short (a few months), based on the isotopic water budget of the marsh in- and outputs ($\delta^{18}O$
159 and δ^2H of H_2O; Delalande et al., 2008a), suggesting a prominent influence of climate in the marsh
160 water budget. The isotopic signature of the marsh water during the humid season (δ^2H-H_2O = -7‰) is
161 close to the mean annual isotopic signature of precipitation recorded at Lwifwa Masoko station (Nivet
162 et al., 2018). At the end of the dry season, the marsh water isotopic signature (δ^2H-H_2O) becomes more
163 ^2H-enriched (between 7 and 16‰, Fig. 1C) demonstrating significant evaporation resulting from the

drier climatic conditions. The slopes of the crater are steep and covered by Zambezian-type (Miombo) forest, dominated by *Brachystegia*, *Uapaca* and *Acalypha* tree species, all common to the region (White, 1983). Shrubs of Rubiaceae and Myriaceae families are present at the edge of the marsh. The vegetation of the marsh is dominated by sedges (*Carex, Cyperus*) while floating (*Nymphaea*) and submerged macrophytes are abundant in the depressions filled with water during the rainy season.

3. Materials and methods

3.1. Core retrieval and sampling

A 4-m long core was collected with a Wright corer in the Kyambangunguru marsh in December 2012. The coring process was stopped at 4 m because of the thickness of the Rungwe Pumice tephra (Fontijn et al., 2012) and thus covers the most recent history of the Kyambangunguru wetland. The core was sampled in 1 cm thick slices at the Lwifwa-Masoko station of University of Dar es Salaam and kept at -20 °C until further treatment. 21 samples were chosen for dating while 35 samples were selected every 12 cm to perform the elemental (carbon and nitrogen content), molecular (br GDGTs, *n*-alkanes) and isotopic (δ^2H_{wax}) analyses. Total organic carbon (C_{org}) and nitrogen (N) contents were determined after decarbonatation by elemental analysis at the Service Central d'Analyse du CNRS, Villeurbanne, France.

105 1 cm-thick samples (ca. every 3 cm) were selected for plant macrofossil analysis. Among these, 44 samples (distributed evenly along the core) were additionally analysed for pollen and non-pollen palynomorphs (NPPs). Within these 44 samples, 12 were used for palynofacies determination. Additionally, 5 surface soil samples (0-5 cm) from the catchment area were collected between the marsh and the top of the crater.

3.2. Absolute chronology and sediment accumulation rate

The chronology of the core is based on 21 Accelerator Mass Spectrometry (AMS) dates performed on bulk Total Organic Matter (TOM; 17 samples) and wood fragments (4 samples; Table 1) all along the core. Samples were subjected to acid-alkali-acid treatment to remove the mineral phase. AMS-^{14}C and

associated $\delta^{13}C$ analyses were conducted on aliquots prepared according to the following AMS protocol: burning at 860 °C for 30 min under vacuum, in the presence of a Cu (II)-oxide/Cu (III)-oxide mix and of Ag string. The obtained CO_2 was graphitized on powdered Fe with H_2 at 650 °C for 100 min, and graphite was compressed in analytical pellets. Residual CO_2 gases were used for associated ^{13}C measurements on a SIRA 10 and are expressed in delta notation per mil versus V-PDB (Vienna Pee Dee Belemnite). Graphite preparation and $\delta^{13}C$ measurements were made at the GEOPS Laboratory (University of Paris-Saclay, France). ^{14}C counting was performed using the AMS facility at the LMC14 laboratory (Laboratoire de Mesure du Carbone 14; Artemis, Saclay; Cottereau et al., 2007). Analytical uncertainties, are ± 0.1‰ for $\delta^{13}C$ and between 0.2 and 0.5 pMC (percentage of Modern Carbon) for ^{14}C activity.

Calibrated radiocarbon ranges were obtained using OxCal 4.3 software (Bronk Ramsey, 2009) with the ShCal13 (Hogg et al., 2013) and Bomb13SH3 (Hua et al., 2013) atmospheric curves as the calibration set (Table 1). A Bayesian age-depth model was used to establish an absolute chronology based on these calibrated ^{14}C date ranges. The age-depth model was constructed applying a *P_Sequence* function, with the parameters k_0=1 and $log_{10}(k/k_0)$=1, in the OxCal v. 4.3 software (Bronk Ramsey, 1995, 2008). Additionally, boundaries reflecting potential changes in the rate of deposit accumulation were introduced to the model, based on observations of micro- and macrofossils (see section 4.5 and 4.6). These boundaries were defined as follows: (i) 417.5 cm: top of the tephra layer and bottom of the model, (ii) 191 cm: abrupt change from lacustrine to marshland conditions, (iii) 115.5 cm: distinct increase in water table and (iv) 0 cm: top of the core. Computing of the age-depth model led to the exclusion of two samples (SacA40028 and SacA38523). Dates with the lowest individual agreement between the modelled and the calibrated date, i.e. SacA40077 and SacA40076, were also excluded from the calculations until the lowest critical value of the agreement index (A_{model}) suggested by Bronk Ramsey (2008) for model reliability (A_{model} = 60%) was achieved. Final A_{model} value of the chronology was 63%. The age is presented as a μ (mean) value of the modelled age expressed as calibrated year before present i.e. AD 1950 (cal. BP; Fig. 2), rounded to tens.

A mean value for the sedimentation accumulation rate (SAR), expressed in cm year^{-1}, was determined as the median value of the probability distribution of the modelled age (μ) for each depth (in cm) at which a date was modelled. The applied formula was the following:

$$\mathrm{SAR} = \frac{1}{\mu_{\mathrm{depth}-0.5} - \mu_{\mathrm{depth}+0.5}} \qquad (1)$$

3.3. Plant macrofossil analysis

About 5 cm^3 of sediment were rinsed with warm water and sieved at 0.25 mm. Macrofossils were studied in transmitted light with a Nikon SMZ800 stereoscopic microscope at a magnification of 10 to 200. Species determination of individual plant macrofossils was performed based on the data from Velichkevich and Zastawniak (2006, 2009). The data were presented as numbers of detected macrofossils and were presented as diagram drawn in the POLPAL software (Nalepka and Walanus, 2003). Analysis was performed at the Adam Mickiewicz University in Poznań (Poland).

3.4. Pollen, non-pollen palynomorphs and microscopic charcoal

Samples for pollen, non-pollen palynomorph and charcoal analysis were prepared using standard laboratory procedures: adding 10% HCl to dissolve carbonates, heating in 10% KOH to remove the humic fraction and at least 24-hour treatment with HF to remove the mineral fraction followed by acetolysis (Berglund and Ralska-Jasiewiczowa, 1986). *Lycopodium* tablet of known number of spores (n=20848, produced by Lund University) was added to each sample for calculation of microfossil concentration (Stockmarr, 1971). Pollen and spores were counted with a biological microscope under 400× and 1000× magnification until the number of at least 500 pollen grains was obtained (Vincens et al., 2003, 2007). Pollen grains were identified using atlases (Gosling et al., 2013), internet-based databases such as African Pollen Database (http://apd.sedoo.fr/), and the Universal Pollen Collection (Institut des Sciences de l'Évolution Montpellier; http://www.palyno.org/). Non-pollen palynomorphs (NPPs) were identified using available literature (Gelorini et al., 2011; Miola, 2012; van Geel et al.,

242 2011). The NPP type numbers follow the convention of 'HdV-number' and 'UG-number', in which
243 acronym 'HdV' means Hugo de Vries Laboratory of the University of Amsterdam (The Netherlands),
244 whereas 'UG' is Universiteit Gent (Belgium) (Miola, 2012). Percentages of pollen grains originating
245 from forest and savannah communities were calculated as the ratio of an individual taxon and the TPS
246 (total pollen sum); the TPS consists of the sum of AP (arboreal pollen) and NAP (non-arboreal pollen
247 but excludes any taxa originating from aquatic and wetland plants as well as spores and NPPs).
248 Percentages of aquatic and wetland pollen taxa, as well as spores and NPPs, were calculated as the ratio
249 of an individual taxon or NPP type and the TPS enlarged by this taxon or NPP type.

250 Microscopic charcoal particles (size range 0.02-0.5 mm) were counted on the same microscopic slides
251 as the ones used for pollen counting until the total number of charcoal particles and *Lycopodium* spore
252 standard was at least 200 in each sample (Finsinger and Tinner, 2005). Values are expressed as the
253 charcoal accumulation rate (CHARmicro) in grains cm^{-2} $year^{-1}$ and were calculated based on the
254 following formula proposed by Davis and Deevey Jr.(1964):

255 $$CHAR_{micro} = CHAC_{micro} \times SAR \quad (2)$$

256 where $CHAC_{micro}$ is the concentration of microscopic charcoal particles (in grains or particles cm^{-3}) and
257 SAR is the sediment accumulation rate (in cm $year^{-1}$). The diagrams were prepared using the POLPAL
258 software (Nalepka and Walanus, 2003) and the analyses were performed at the Adam Mickiewicz
259 University in Poznań (Poland).

260

261 3.5. Quantitative palynofacies analysis

262 Sample preparation included treatment with 50 ml of HF overnight at 40°C followed by 50 ml of HCl
263 for 30 min to eliminate siliciclastic and carbonate minerals. Samples were then rinsed until neutral pH.
264 Quantification of the different types of organic matter (OM) is based on the methodology developed by
265 Graz et al. (2010) using incorporation of a standard solution of *Cupressus* pollen at 10 $mg.ml^{-1}$ in each
266 sample. Samples were prepared in thin sections before optical investigations using a transmitted light
267 microscope with a 50× magnification. Particle identification was performed using the methodology

described by Boussafir et al. (2012) and Graz et al. (2010). Particles were classified into 3 types: (i) Ligno-Cellulosic tissues (LC) at different stages of degradation comprising fresh tissues detected as translucent LC (tLC), slightly degraded/amorphised LC (saLC) with cell structures that are still partially recognizable and totally degraded/amorphous LC, characterised by red aggregates of amorphous OM (rAOM) as originally described by Graz et al. (2010), (ii) mycelium fragments (myc; Graz et al., 2010) and (iii) planktonic remains (algal organic matter, algOM; Boussafir et al., 2012). Whenever necessary, particle identification was aided using UV excitation. The total mass of each particle type was determined after 40 counting according to Eq. 3:

$$m_{part} = \frac{m_{std} \times A_{part}}{A_{std}} \times \frac{d_{part}}{d_{std}} \qquad (3)$$

with m_{part}: mass of the particle; m_{std}: mass of the standard; A_{part}: counted surface of the particle; A_{std}: counted surface of the standard; d_{part}: density of the particle; d_{std}: density of the standard. Densities used for the calculation were determined by Graz et al. (2010). Results are expressed as relative abundance (in terms of mass) of each particle to the total. Sample preparation and analysis were performed at the University of Orléans (France).

3.6. Biomarker analyses

3.6.1. Lipid extraction

After freeze-drying, samples were submitted to a modified Bligh-Dyer extraction as described in Coffinet et al. (2015). The total lipid extract was then separated into three fractions on a silica column with a succession of (i) DCM, (ii) DCM:acetone (2:1, v:v) and (iii) DCM:MeOH (1:1, v:v) followed by pure MeOH as solvents (Coffinet et al., 2015). The apolar fraction containing the *n*-alkanes and the intermediate polarity one (fraction 2) containing the GDGTs were analysed. Prior to analysis, the apolar fraction was further separated on silver nitrate impregnated silica columns (10%, w:w) in Pasteur pipettes (with heptane and then DCM as eluents) in order to purify the linear *n*-alkanes for compound-specific δ^2H analysis.

293 *3.6.2. n-Alkane analyses*

294 *n*-Alkanes were analysed at Sorbonne University (Paris, France) by gas chromatography coupled to a
295 mass spectrometer (GC-MS) using an Agilent Network 6890 GC System coupled with a 5973 Mass
296 Selective Detector, with electron impact at 70 eV. 1 µl was injected and separation was achieved using
297 a Restek RXI-5 Sil MS silica capillary column (30 m × 0.25 mm i.d., 0.50 µm film thickness) with He
298 as the carrier gas at 1 ml min^{-1} flow rate. Initial temperature was set at 50 °C and increased to 320 °C at
299 4 °C min^{-1}. Samples were injected in splitless mode and the injector temperature was 280 °C.

300 The average chain length (ACL; Eq. 4) describes the *n*-alkane distribution profile of a sample and is
301 used to determine the predominant origin of the *n*-alkanes. Typically, *n*-alkanes with chain with less
302 than 21 carbon atoms are suggested to be produced by algae and cyanobacteria (e.g. Han et al., 1968)
303 while *n*-alkanes with more than 25 carbon atoms more likely originate from terrestrial higher plants
304 (Eglinton and Hamilton, 1967). *n*-Alkanes with chain length between 21 and 25 carbon atoms are
305 predominantly found in aquatic macrophytes (Ficken et al., 2000).

306 $$\mathrm{ACL}=\frac{\sum C_i \times i}{\sum C_i} \quad \text{where } i \text{ spans from 21 to 35} \qquad (4)$$

307 The carbon preference index (CPI; Eq. 5) is a ratio assessing the relative importance of odd over even
308 homologues and reflects the degree of maturity (organic matter degradation) of a sample. Immature
309 samples have very high CPI (>> 1; Killops and Killops, 2005). Unusually low CPI (below 3) in recent
310 sediments are generally considered as polluted by a source of mature organic matter (petroleum, wood
311 burning; Bray and Evans, 1961).

312 $$CPI = 0.5 \times \left(\frac{\sum C_{odd\ 25-33}}{\sum C_{even\ 24-32}} + \frac{\sum C_{odd\ 25-33}}{\sum C_{even\ 26-34}}\right) \qquad (5)$$

313 The P_{aq} index (Eq. 6) was developed by Ficken et al. (2000) and is a proxy for the relative contribution
314 of emergent/terrestrial macrophytes compared to submerged/floating ones. Contribution of submerged
315 and floating macrophytes is considered as high when P_{aq} values are higher than 0.4 and insignificant
316 when P_{aq} values are lower than 0.1.

317 $$P_{aq} = \frac{C_{23}+C_{25}}{C_{23}+C_{25}+C_{29}+C_{31}} \qquad (6)$$

318 *n*-Alkane hydrogen isotopic composition (δ^2H *n*-alkane) was measured at Newcastle University (United-
319 Kingdom) using a Delta V+ isotope-ratio mass spectrometer (IRMS, Thermo Fisher) connected to a GC
320 Ultra Trace (Thermo Fisher), a Finnigan GC Combustion III (Thermo Fisher) and a high temperature
321 conversion (HTC) system set up at 1400 °C. The GC temperature was set to start at 50 °C and then to
322 raise to 250 °C at 15 °C min^{-1} and from 250 °C to 320 °C at 5°C min^{-1}. Temperature was then held at
323 320 °C for 15 min. Every sample was analysed in duplicate and the $^2H/^1H$ ratio was reported on the V-
324 SMOW (Vienna standard mean ocean water) scale and expressed in delta per mil (δ‰). A mixture of
325 *n*-C_{16} to *n*-C_{30} alkane standard and 5α androstane standard (A. Schimmelmann, Indiana University) was
326 run at the beginning and at the end of each sequence. Standard error of the measurements of the
327 individual long chain *n*-alkanes (C_{23}-C_{31}) from this standard mix ranged between 0.3‰ and 1.1‰.

328 *3.6.3. GDGT analysis*

329 GDGTs were analysed at Sorbonne University (Paris, France) with a high-pressure liquid
330 chromatography coupled to a mass spectrometer with an atmospheric pressure chemical ionization
331 source (HPLC-APCI-MS, Shimadzu LCMS-2020). Separation was achieved with a Prevail Cyano
332 column (2.1 mm x 150 mm, 3 µm; Alltech, Deerfield, IL, USA) at 30 °C, using a mixture of hexane and
333 isopropanol at 0.2 ml min^{-1} according to Coffinet et al. (2015). Elution began at 99% A/1% B for 5 min
334 followed by a linear gradient to 98% A/2% B in 45 min. A second linear gradient led to a mixture of
335 90% A/10% B in 10 min, maintained for 10 min and returned to the initial conditions (99% A/1% B) in
336 14 min, maintained for 10 min. Injection volume was 10 µl. Single ion monitoring (SIM) of the $[M+H]^+$
337 ions was used to detect the GDGTs.

338 Mean annual air temperatures (MAAT) were estimated using the calibration specifically developed for
339 East African lakes by Loomis et al. (2012):

340 $$MAAT = 22.77 - 33.58 \times f(III) - 12.88 \times f(II) - 418.53 \times f(IIc) + 86.43 \times f(Ib) \quad (7)$$

341 where *f*(x) is the fractional abundance of the compound x relative to the total br GDGTs and the roman
342 numerals correspond to the different br GDGT compounds according to Weijers et al. (2007b)
343 numbering.

pH was calculated using the soil calibrations developed by Tierney et al. (2010b) and based on the cyclisation ratio of br GDGTs (CBT; Weijers et al., 2007b):

$$pH = 10.32 - 3.03 \times CBT \quad (8)$$

$$CBT = -\log\left(\frac{[Ib]+[IIb]}{[I]+[II]}\right) \quad (9)$$

where the roman numerals correspond to the different br GDGT compounds according to Weijers et al. (2007b) numbering.

4. Results

4.1. Lithology

The bottom of the core corresponds to a pumice-rich tephra. The overlaying deposits (ca. 418 to 200 cm) consist of an alternating layer of peat, organic gyttja and silty clay material, with charcoal-rich layers (Fig. 2). Above 200 cm, the sediment mostly consists of peat at diverse stages of decay. Large amounts of higher plant macrofossils are observed at depth ranging between 175 and 75 cm, while the decomposition of plant fragments is more pronounced from 75 cm to the top of the sequence. The upper clayey part of the sequence contains two additional tephra layers at 65.5-63 cm and at 57-51 cm (Fig.2).

4. 2. Chronostratigraphy, age-depth model and sedimentation accumulation rate

As shown in Table 1 and Figure 2, dates were obtained all along the core and generally fit with the stratigraphy. Nevertheless, two age reversals are observed at the base of the core, based on Total Organic Matter (TOM) measurements (Fig. 2). The first one occurs between 371.5 and 402 cm depth (SacA44028) and the second corresponds to the bottom tephra layer of the core between 417.5 and 420.5 cm depth (SacA38523; Table 1). This could be attributed to stratigraphic misplacement or cross-contamination during coring. Therefore, these dates were not included in the age model. All the wood remain-based ages are very close to those from bulk TOM or slightly older (mean standard deviation

between the bulk TOM and the wood remain age is +2.3%). This minor mismatch could be due to the additional transport time of the wood remains from the catchment into the marsh sediment while the bulk TOM signature is expected to be predominantly autochthonous (see sections 4.4 to 4.6). Alternatively, "younger" TOM ages could result from microbial activity or organic matter derived from root development occurring after sedimentation (Trumbore, 2009). The $\delta^{13}C$ values obtained after sample preparation on residual CO_2 vary from -20.0‰ to -29.5‰ along the core (average value -25.3‰; Tab. 1). This range is compatible with organic carbon originating from the vegetation, likely C3 type plants, and consistent with $\delta^{13}C$ values measured at the nearby Lake Masoko (Gibert et al., 2002). Compared to the mean TOM $\delta^{13}C$ value (-24.8‰), the mean wood $\delta^{13}C$ value is lower (-27.2‰) also in agreement with a C3 type plant signature.

The investigated sediment sequence from Kyambangunguru shows continuous sedimentation of ca. 4080 calibrated years, spanning from ca. 4020 and -60 cal. BP (Fig. 2). The "apparent" sediment accumulation rate (SAR) ranges from 0.03 to 0.18 cm yr^{-1} (i.e., each cm thick sample of the profile records 6.3 to 33 years). The highest SAR was recorded in the bottom section of the profile (between 0.10 and 0.18 cm yr^{-1}), in the 417-191 cm section (from 4015 to 2280 cal. BP). Intermediate SAR values, ranging between 0.07 and 0.11 cm yr^{-1}, were recorded between 191 and 8 cm (from 2280 to 130 cal. BP), whereas the lowest SAR (0.03-0.06 cm yr^{-1}) was recorded in the top section of the profile between 8 and 0 cm (from 130 to -60 cal. BP). The σ error of the modelled dates ranged between 0.2 (top of the profile) and 53 years.

4.3. Palynofacies

The Kyambangunguru core is largely dominated (ca. 80% of the OM throughout the core) by ligno-cellulosic tissues (LC) from vascular plants (Fig. 3). Microscopic investigation of the LC reveals 3 stages of degradation. On average, fresh, well-preserved, tLC tissues represent 19% of the total OM (Fig. 3), while slightly degraded, saLC particles are the most abundant type of OM (ca. 39% on average) in the core. Amorphous rAOM represents ca. 11% of the total LC OM with an increase to 20% in the section from ca. 3140 to 830 cal. BP (300-62.5 cm). In addition to LC, fungal mycelia are observed in the layer

spanning the period between 239 and 60 cm (ca. 2670 to 800 cal. BP). Grey cell fragments and granular amorphous OM, related to planktonic-derived material, are found throughout the core (Fig. 3), but are particularly abundant at the base (below 330 cm, i.e. ca. 3360 cal. BP) and at the top of the profile (from 89.5 to 0 cm, ca. 1150 cal. BP to modern).

4.4. Plant macrofossil analysis

Plant macrofossils are dominated by macrophytes (sedges, submerged/floating plants and algae) and wood remains. *Eleocharis* sp. is present all along the core, while *Nymphaea* sp. (floating macrophyte), disappeared between 160 and 100 cm (ca. 1960 and 1270 cal. BP; Fig. 4). In addition, in the layer between 415.5 and 281.5 cm (ca. 4000 to 3000 cal. BP), macrofossils are composed of remains of algae (*Nitella* sp., Fig. 4) and submerged/floating plants (*Potamogeton* sp. and *Caldesia parnassiflora*; Fig. 4). These species are replaced by *Juncus* sp. from 239.5 to 139.5 cm (ca. 2670 to 1730 cal. BP). During this interval, there is a relative increase in abundance of wood remains in comparison to the other sections of the core. *Nitella* sp. together with *Carex* sp. and *Chara* sp. are the dominant remains found in the sequence from 139.5 to the surface (1730 cal. BP to modern; Fig. 4). At 105 cm (ca. 1330 cal. BP), *Aldrovanda vesiculosa* seed was found.

4.5. Pollen, NPPs and microcharcoal

265 taxa of pollen and spores as well as non-pollen palynomorphs (NPPs) – organic walled microfossils which are not pollen – were identified by palynological analysis. The results of this analysis were separated into two groups: indicators of terrestrial vegetation, i.e. vegetation surrounding the lake/marsh and indicators of aquatic vegetation reflecting mainly lake-marsh vegetation. Three pollen zones reflecting compositional changes in terrestrial (woodland and open land) communities (labelled as KY/tp-1 to -3 with tp: terrestrial pollen; Fig. 5) were defined. Additionally, the KY/tp-1 zone was subdivided into three subzones (KY/tp-1a-c). Pollen and NPPs reflecting lake/marsh vegetation changes enabled the establishment of 6 zones (KY/lpn-1-6 with lpn standing for local pollen and NPPs; Fig. 6).

421 *4.5.1. Terrestrial vegetation*

422 The KY/tp-1 zone (416–303 cm; ca. 4000–3160 cal. BP) is characteristic of the highest percentages of
423 *Acalypha*, Moraceae, *Macaranga* and *Piptadenia*/*Piptadeniastrum*/*Entada* (Fig. 5). Moraceae and
424 *Macaranga* pollen reached their maxima (27–28% and 11%, respectively) at 353-333 cm (ca. 3520–
425 3380 cal. BP). Poaceae pollen increased until 397 cm (ca. 3850 cal. BP) when they distinctly decreased
426 while Proteaceae pollen revealed a first maximum at 378 cm (ca. 3700 cal. BP). During the KY/tp-1b
427 subzone (353–333 cm; ca. 3520–3380 cal. BP), Poaceae percentages fell to their minimum values (8%).
428 During the KY/tp-1c subzone (333–303 cm; ca. 3380–3160 cal. BP) pollen values of Moraceae and
429 *Macaranga* dropped simultaneously with the rise in Poaceae percentages and the appearance of palm
430 pollen (*Elaeis guinensis* and *Raphia* type). During the entire KY/tp-1 zone charcoal (0.02–0.5 mm),
431 accumulation rate (CHAR) was high and relatively stable without any distinct maximum (8450–37940
432 particles cm^{-2} yr^{-1}; Fig. 5).

433 The KY/tp-2 zone (303–63 cm; ca. 3160–830 cal. BP) was characteristic of the highest values of *Uapaca*
434 (15–24%; 162.5-133.5 cm; ca. 1990–1660 cal. BP) in the profile. However, at 123–113.5 cm (ca. 1540–
435 1430 cal. BP) they substantially declined, simultaneously to a rapid increase in Poaceae values. At the
436 beginning of the zone, *Raphia* pollen increased rapidly (303–283 cm; ca. 3160–3010 cal. BP; up to
437 15.5%). Values of Proteaceae increased from 234.5 cm (ca. 2630 cal. BP) and reached the maxima after
438 113.5 cm (ca. 1430 cal. BP). Simultaneously, or slightly prior to the Poaceae maximum in this zone
439 (123–113.5 cm ca. 1540–1430 cal. BP), values of *Ricinus communis* and *Macaranga* increased (142.5
440 cm; ca. 1760 cal. BP), whereas percentages of *Nauclea* type (123 cm; ca. 1540 cal. BP), *Elaeis guinensis*
441 (143 cm; ca. 1770 cal. BP), *Raphia* type (132.5 cm; ca. 1650 cal. BP) and later Rutaceae (113.5 cm; ca.
442 1430 cal. BP) decreased substantially or disappeared. Among pollen taxa related to arboreal plants
443 occupying montane forest zones, *Apodytes* cf. *dimidiata*, *Olea*, *Podocarpus* and *Prunus africana* type
444 were the most common. During the KY/tp-2 zone, three distinct phases of increase in CHAR values,
445 potentially related to an increase in fire activity, were identified. These occurred at 297.5, 248.5 and
446 117.5 cm (ca. 3120, 2740, and 1480 cal. BP respectively) and were intersected by periods with CHAR

values lower than during the KY/tp-1 zone. From 83 cm (ca. 1070 cal. BP), CHAR values started to increase gradually.

The KY/tp-3 zone (63–5 cm; 830 to 60 cal. BP) was characterized by the highest percentages of Poaceae (67–90%), the continuous presence of *Ricinus communis* and distinct drops of Proteaceae and *Uapaca*. At 50 cm (ca. 690 cal. BP), *Syzygium* pollen value revealed a substantial increase (up to 16%). In general, CHAR values were higher than in the previous zone and two distinct maxima of their values were recorded at 50 and 10 cm (ca. 690 and 160 cal. BP).

4.5.2. Aquatic/marsh vegetation

During the KY/lpn-1 zone (416–383 cm; ca. 4000–3740 cal. BP) the algae *Tetraedron trigonum* type, *Tetraedron incus/caudatum* and *Coelastraum reticulatum* reached their maxima (Fig. 6). These algae taxa rapidly declined between 412 and 393 cm (ca 3970 and 3820 cal. BP). Along the KY/lpn-2 zone (383–303 cm; 3740–3160 cal. BP), Alismataceae (cf. *Caldesia*) was regularly observed (0.8–6.5%). Pollen of Nymphaeaceae (*Nymphaea* type) and their epidermis (UG-1241), *Potamogeton* and algae such as *Scenedesmus*, *Tetraedron minimum*, *Pediastrum* undiff., *Pediastrum angulosum* and *Botryococcus* were frequent during these two zones. At 323 cm (ca. 3310 cal. BP), *Nymphaea* type percentages increased simultaneously with a decline in *Potamogeton*. The KY/lpn-3 zone (303–193 cm; ca. 3160–2300 cal. BP) was characterized by an increase in Cyperaceae pollen and tissue fragment percentages (rise in fungal NPP UG-1176 and UG-1197) and a simultaneous drop in *Scenedesmus* and *Tetraedron minimum.*

The KY/lpn-4 zone (193–113 cm; ca. 2300–1430 cal. BP) was characterized by a prominent increase in Cyperaceae percentages (12–77%). The spores of *Lycopodiella caroliniana* were regularly present (0.2–18%) together with amoeba *Assulina muscorum*. Between 143 and 123 cm (ca. 1770 and 1540 cal. BP), monolete spores reached their maximum values in the core (64–69%). Values of *Nymphea* type, UG-1241 (*Nymphaea* tissues), *Potamogeton*, Alismataceae (cf. *Caldesia*), *Pediastrum angulosum*, *Botryococcus* and *Scenedesmus* dropped markedly. NPPs of fungal origin increased distinctly, notably UG-1197 and *Entorrhiza* in the deeper part of the zone and HdV-172, UG-1077, UG-1176 and UG-1107 in the upper part.

474 The KY/lpn-5 (113–46.5 cm; ca. 1430–650 cal. BP) and KY/lpn-6 (46.5–5 cm; 650 to 60 cal. BP) zones
475 were characterized by the increase in frequency of algae, mainly *Botryococcus*, *Scenedesmus* and
476 *Pediastrum angulosum* and, among submersed macrophytes, of *Nymphaea* type pollen and their related
477 tissues (UG-1241). In the KY/lpn-5 zone, Hallorrhagaceae appeared (1.5–24%). *Entorrhiza* and fungal
478 type UG-1107 reached maxima in the profile (59–76%). In the KY/lpn-6 zone, Alismataceae (cf.
479 *Caldesia*) and *Potamogeton* became more frequent while Cyperaceae pollen percentages distinctly
480 dropped.

481

482 4.6. Elemental analysis

483 C_{org} content is high throughout the core (39.0 - 57.8%; mean 51.0% ± 6.2; Suppl. Table 1), except in the
484 tephra layer at the base of the core (5%). Total nitrogen (TN) varies from 1.5 to 3.6% except for the
485 tephra layer (0.2%). Slightly lower TN values are observed between 199.5 and 100 cm (ca. 2350 and
486 1270 cal. BP; ca. 2%, Suppl. Table 1) leading to higher C/N ratios that range from 16 to 38 (Fig. 7 and
487 Suppl. Table 1). In the other sections of the core, C/N ratios are relatively invariant at ca. 15.

488

489 4.7. Br GDGT abundance and distribution

490 Br GDGTs are abundant throughout the core (mean 121.5 ± 81.3 μg g^{-1} of dry wt. peat), with maximal
491 concentration observed at 150.5 cm (ca. 1850 cal. BP; Suppl. Table 1). CBT varies between 0.53 and
492 2.01 with a mean value of 1.31 and is higher above 180.5 cm (ca. 2180 cal. BP; 1.41-2.01; Suppl. Table
493 1). MBT is comprised between 0.65 and 0.89, with a mean value of 0.77 (Suppl. Table 1). The highest
494 MBT values (>0.80) are found between 194 and 45 cm (ca. 2310 and 630 cal. BP).

495

496 4.8. *n*-Alkane distribution and their δ^2H composition

497 Mid- to long-chain *n*-alkanes (>C_{21}) dominate most of the samples, with C_{23} and C_{25} being the most
498 abundant (on average 23% and 21%, respectively; Suppl. Fig. 1). Two *n*-alkane distribution patterns are

observed in the core (Suppl. Fig. 1), defined as patterns A and B. Pattern A was identified in the sections from 417 to 180 cm and from 30 cm to the surface (ca. 3670 -2300 cal. BP and ca. 430 cal. BP-modern respectively). It is dominated by odd numbered *n*-alkanes, the most abundant one being C_{23}, with a decreasing trend in relative abundance from C_{23} to C_{31}. Pattern B (Suppl. Fig. 1) was observed in the sections from 193 to 29.5 cm (ca. 2300 to 430 cal. BP). This distribution is characterized by a flattening of the *n*-alkane profile. The C_{29}^{+} *n*-alkanes (up to C_{35} in some samples) as well as the C_{23}^{-} *n*-alkanes, especially C_{19}, increase while the C_{23}, C_{25} and C_{27} decrease, in comparison to pattern A. In pattern B, even numbered *n*-alkanes are also found in larger amount than in pattern A.

The CPI index confirms a strong odd-over-even predominance throughout the core (mean 8.1±3; Suppl. Table 2) while the ACL index varies between ca. 25 and 27 (Fig. 7; Suppl. Table 2). The P_{aq} index is systematically higher than 0.4, ranging between 0.50 and 0.85 (Fig. 7; Suppl. Table 2).

The δ^2H values of odd mid to long chain *n*-alkanes (C_{23}-C_{31}) varies between -96‰ and -172‰ (Suppl. Table 2) and are higher in the deepest part of the core, between 417 and 391 cm (ca. 4010 and 3800 cal. BP; between -96‰ and -122‰; Suppl. Table 2). Long chain *n*-alkanes (C_{29} and C_{31}) are more ^2H-enriched (-130‰ on average; Suppl. Table 2) than mid chain (C_{23} and C_{25}; -150‰ on average; Suppl. Table 2) compounds.

5. Discussion

The combination of palaeobotanical, elemental and molecular analyses enabled the reconstruction of the Holocene ecological history of the Kyambangunguru wetland together with regional climate. The proxy analyses revealed the presence of three major phases in the Kyambangunguru wetland ecosystem development over the last 4.0 ka cal. BP for which the interaction with regional and global climatic changes are discussed. The chronology of the sediment record was compared to published records of the region (Filippi and Talbot, 2005; Fontijn et al., 2012; Garcin et al., 2007) showing overall good consistency. The tephra layer at the base of the core, dated at ca. 4.1 ka cal. BP, corresponds to the Rungwe Pumice deposits identified at Lakes Masoko and Malawi and dated at 4.3 ka cal. BP and 4.3 to

525 3.6 ka cal. BP, respectively. The second tephra observed at ca. 0.9 ka cal. BP in the Kyambangunguru
526 core can be related to the Aphyric Pumice deposits observed at 1.2 ka cal. BP in the Lake Masoko
527 sediment record and between 1.1 and 0.6 ka cal. BP in the Lake Malawi one. The last tephra layer
528 identified at Kyambangunguru is harder to define. It is dated at ca. 0.8 ka cal. BP and could either
529 correspond to the Aphyric Pumice described earlier or to the Ngozi Tuff, even though this event was
530 dated between 0.5 and 0.3 ka cal. BP at Lakes Masoko and Malawi. This regional comparison, even if
531 it stresses its inherent time uncertainty, further validates the age-model used in this study.

532

533 5.1. Ecosystem, air temperature and precipitation variability at the Kyambangunguru crater marsh

534 Three units (labelled as Units I-III; Fig. 7), representing the major developmental phases of marshland
535 ecosystem over the last 4.0 ka cal. BP, were distinguished based on the local plant community changes
536 inferred from pollen, non-pollen palynomorph and plant macro-fossil analyses. In addition, the origin
537 of the OM and its degree of preservation were determined using the palynofacies and C/N records
538 (Bourdon et al., 2000) while the distribution of br GDGTs allowed reconstructing the pH of the site,
539 following the approach described by Weijers et al. (2007b) and Tierney et al. (2010b). For the climatic
540 reconstruction, the mean annual air temperature (MAAT) and the hydrological conditions over the last
541 4.0 ka cal. BP years were reconstructed using the br GDGT distribution and the hydrogen isotopic values
542 of the *n*-alkanes (δ^2H_{wax}), respectively. Br GDGT-derived MAAT were calculated with the East African
543 lacustrine calibration developed by Loomis et al. (2012), i.e. Eq. 7, which takes into account *in situ*
544 production of br GDGTs in lakes, as discussed in the Suppl. Information. The δ^2H_{wax} was determined as
545 the weighted average of the δ^2H values of the C_{23} and the C_{25} *n*-alkanes which are expected to have
546 recorded mainly the wetland water isotopic composition (δ^2H-H_2O) variations during the accumulation
547 of the sedimentary sequence (as discussed in the Suppl. Information). Because the study site has no
548 outflows, the δ^2H-H_2O variations depend essentially on the rates of precipitation and evaporation and
549 the δ^2H_{wax} can be interpreted as changes in the precipitation to evaporation ratio (P/E ratio; Gonfiantini,
550 1986; Sachse et al., 2004).

551

552 *5.1.1. Unit I: ca. 4.0 – 2.3 ka cal. BP (417–193 cm) – shallow lake, cold and wet conditions*

553 The palaeoenvironmental proxies suggest a relatively stable and persistent lake environment during this
554 period. Planktonic remains are observed in the palynofacies (Fig. 3) and in the non-pollen palynomorph
555 profile (NPP; Fig. 6) and the C/N values (ca. 15; Fig. 7) indicate a mixed aquatic and terrestrial source
556 of the OM (Meyers, 1997). The GDGT derived-pH of ca. 7 (Fig. 7) is consistent with current pH values
557 of the RVP crater lakes (ranging between 5.8 and 8.7; Delalande, 2008), further supporting the
558 occurrence of a lake at this time. The high abundance of macro- and microremains (Figs. 4 and 6) from
559 algae (*Nitella* sp.) and submerged/floating macrophytes (*Potamogeton* sp. and *Nymphaea* sp.) and the
560 relatively high P_{aq} values (0.7-0.8; Ficken et al., 2000) suggest that the lake was relatively shallow and
561 its water column likely harboured abundant macrophyte vegetation. The growth of *Caldesia*
562 *parnassifolia* for instance may indicate a water depth lower than one meter (Gupta and Beentje, 2017;
563 Sinkevičienė, 2016). In addition, the NPP record reveals a characteristic pattern of successive and rapid
564 decline of *Tetraedron trigonum* type, *Coelastrum reticulatum* and *Tetraedron incus*/*caudatus*, all before
565 3.8 ka cal. BP (Fig. 6). This reduction is possibly related to the spread of *Nymphaea* whose floating
566 leaves may have limited the light availability, although it did not seem to impact *Tetraedron minimum*
567 and *Scenedesmus*, which might be more resistant species. The second stage of microalgal community
568 retreat, which affected *Scenedesmus* and *Tetraedron minimum*, occurred at ca. 3.2 ka cal. BP and seem
569 to have also been stimulated by *Nymphaea* expansion. Simultaneously, an increased input of fungal
570 remains, UG-1176 and UG-1197, may indicate spreading of emerged marsh plants around the lake. This
571 is further supported by the high C_{org} values (> 50%; Suppl. Table 1) and the predominance of
572 lignocellulosic-derived OM in the palynofacies record partly originating from *Cyperus* (Laggoun-
573 Défarge et al., 2008a) according to microscopic observation (Fig. 3).

574 Unit I is marked by an abrupt decrease in mean annual air temperature (MAAT) of about three degrees
575 (from 26 °C to 23 °C, Fig. 8) at ca. 3.9 ka cal. BP. The MAAT continues to decrease by another three
576 degrees to 20 °C at 2.7 ka cal. BP (Fig. 8). This trend is synchronous with the "3.3–2.5 ka. BP" cold
577 Holocene event introduced by Wanner et al. (2011) which was also observed – to a lower extent – at ca.

4.0 – 3.0 ka cal. BP in Lakes Tanganyika and Malawi (Powers et al., 2005; Tierney et al., 2008; Fig. 8) and in Lakes Turkana and Challa (Berke et al., 2012;

Sinninghe Damsté et al., 2012). At the same time, the δ^2H_{wax} record shows more negative values until ca. 3.0 ka cal. BP (up to -168 ‰; Fig. 9), which can be interpreted as an increase in the P/E ratio either due to higher precipitation or/and lower evaporation rates. A wetter environment is also inferred from the terrestrial pollens, with a decrease in pollen supply from grassland communities from ca. 3.7 to 3.4 ka cal. BP and an expansion of mountain forest and Zambezian Miombo woodland communities (Moraceae and *Macaranga* at ca. 3.5 – 3.4 ka cal. BP, *Uapaca* optimum, presence of *Apodytes cf. dymidata*, *Olea*, *Podocarpus* and *Prunus africana).* Wetter conditions at the same period were also inferred from a pollen record at Lake Masoko (Vincens et al., 2003). Notably, a synchronous *Uapaca* pollen optimum occurred both at Masoko and Kyambangunguru (after ca. 3.1 ka cal. BP, Vincens et al., 2003). δ^2H_{wax} values remain negative during unit I, although two positive peaks in δ^2H_{wax} are noticeable at ca. 3.6 and 2.8 ka cal. BP possibly indicating brief dry events interrupting the overall wetter period. These dry events are in agreement with observations by Russell et al. (2003) and Russell and Johnson (2005) at Lake Edward (Uganda; Fig. 9). Peaks in Mg content in calcite at 3.6 and 2.8 ka cal. BP were indeed linked to evaporative concentration of the lake (increase in the $[Mg^{2+}]/[Ca^{2+}]$ ratio in lake water) in response to short but pronounced drought events.

5.1.2. Unit II: 2.3 – 1.4 ka cal. BP (193–113 cm) – marsh/peatland formation under sustained warm and drier conditions

An abrupt, environmental change occurred at ca. 2.3 ka cal. BP leading to the establishment of a peatland with variable hydrological conditions (Fig. 7). The onset of unit II is marked by an apparent decrease in the sedimentation rate from 0.13 cm yr^{-1} to 0.08 cm yr^{-1} (Fig. 2), an increase in the Cyperaceae tissue and ferns (monolete spores) accumulation and a strong increase of the C/N ratio (up to 40), all evidencing peat soil formation. High C/N ratios (usually > 30 and sometimes up to 100) are indeed typical for peatlands, due to the high preservation of the OM in relation to the prevailing acidic and anoxic conditions (Laggoun-Défarge et al., 2008b; Meyers, 1997). Simultaneously, a substantial decrease or almost total disappearance of algae (*Scenedesmus*, *Pediastrum*, *Botryococcus* and

Tetraedron minimum) and aquatic plants such as *Nymphaea* spp. (Fig. 6) reflect a substantial fall in the water table. However, irregular appearances of these taxa, as well as of the macroalgae *Nitella sp.*, indicate episodic inundation of the wetland (Fig. 4). The main constituents of the peatland community were *Juncus* sp., *Eleocharis* sp., ferns and perhaps other Cyperaceae species (Figs. 4 and 6). Permanent waterlogged conditions, and low pH (down to 5.2, Fig. 7) contributed to the establishment of plant taxa restricted to humid acidic environments, such as *Drosera*, *Lycopodiella caroliniana* and *Aldrovanda vesiculosa* (Figs. 4 and 6; (Gałka et al., 2015), and the appearance of protists frequently found in peatlands, such as the testate amoeba *Assulina muscorum* (van Geel, 1978). The increase in reddish amorphous OM (rAOM) and the appearance of fungal mycelia at that time (Fig. 3) also suggest the start of a terrestrialization process and the development of vascular plants within the marsh (Bourdon et al., 2000). The increase in wood remains in the macrofossil profile, related to the development of trees and shrubs at the edges of the marsh or even in the marsh itself, supports this interpretation.

Unit II displays the highest δ^2H_{wax} values of the core (up to -136 ‰; Fig. 9), suggesting low P/E ratio and thus the driest period of the last 4.0 ka cal. BP, consistent with several East-African records – Lake Edward (Uganda), Lake Turkana (Kenya), Lake Tanganyika (Tanzania) (Nash et al., 2016 and references therein). A major drought event is widely described at ca. 2.0 ka cal. BP, followed by a second period between ca. 1.7 and 1.0 ka cal. BP, during which successive minor drought events occurred (Alin and Cohen, 2003; Russell et al., 2007; Russell and Johnson, 2005; Verschuren and Charman, 2008). In the Kyambangunguru δ^2H_{wax} record, a positive excursion that could be interpreted as a drought event is observed at ca. 2.2 ka cal. BP. However, the major dry period seems to have occurred later, between ca. 1.7 and 1.4 ka cal. BP (centred at 1.5 ka cal. BP, Fig. 9). Around the same time (ca. 1.7 ka cal. BP), *Uapaca* pollen suddenly declined and fire activity increased, which contributed to the opening of the woodland canopy and a spread of the grassland communities (Fig. 5). The same abrupt changes are noticeable in charcoal and pollen data at Lake Masoko (Thevenon et al., 2003; Vincens et al., 2003) and in the Amboseli basin in Kenya (Rucina et al., 2010). Alternatively, these vegetation changes could have been induced by enhanced human activity. Indeed, a first spread of human settlement is considered to have occurred during the Late Iron Age, around 1.5 ka cal. BP (Marchant and Taylor, 1998; Vincens et al., 2003). However, several sites in East Africa (Lakes Turkana, Tanganyika, Naivasha, Challa, Edward

633 and Sacred Lake; see references in Marchant et al., 2018) support a widespread increase in aridity as the
634 main cause explaining the sedimentological evidence of droughts, as discussed by Marchant et al.
635 (2018). Notably, we promote that δ^2H_{wax} records, such as this study and Konecky et al. (2014), could
636 help disentangling the human impact from the climatic one as they should only be marginally impacted
637 by human activities. According to the br GDGT data, MAAT remained high during unit II, oscillating
638 around 21.5-22 °C (Fig. 8), suggesting a dry and warm period during unit II. During the same period,
639 higher temperatures are also reported in the records from Lake Challa (Sinninghe Damsté et al., 2012),
640 Lake Turkana (Berke et al., 2012) and Lake Tanganyika (Tierney et al., 2008) (Fig. 8).

641 *5.1.3. Unit III: ca. 1.4 ka cal. BP – modern (113–0 cm) – periodically flooded marsh and*
642 *transition to colder conditions*

643 At the onset of Unit III, an increase in the water table led to the reappearance of microalgae assemblages
644 (mainly composed of *Botryococcus*, *Scenedesmus* and *Pediastrum angulosum*), and macrophytes such
645 as *Nymphaea*, Alismataceae and Hallorrhagaceae at ca. 1.4 ka cal. BP. However, until ca. 0.7 ka cal.
646 BP, high percentages of Cyperaceae and of *Entorrhiza* spores are observed, which indicate that the
647 peatland was subjected to pronounced water table fluctuations but without open water stages. Indeed,
648 *Entorrhiza* is a genus of parasites that infect the roots of the Juncaceae (rush) and Cyperaceae (sedge)
649 families when they are no longer in water (Riess et al., 2015; Vánky, 1998). At ca. 0.7 ka cal. BP, the
650 water table likely increased substantially, which supported a spread of *Nymphaea* and contributed to the
651 sharp decrease in Cyperaceae. Since ca. 0.4 ka cal. BP, *Tetraedron minimum* and *Scenedesmus* blooms
652 became more frequent, and the structure of the microalgal communities resembled the one from the base
653 of the core (start of Unit I). This time, however, large amounts of *Carex* remains and large fluctuations
654 in pH (from 5.2 to 7.8; Fig. 7) suggest the coexistence of peat patches, likely acidic, and water
655 depressions where the pH may have been higher, supporting the development of microalgal
656 communities. This corresponds to the current status of the marsh. Continuous monitoring of the site
657 during the last decade indicates the presence of a seasonally evolving ecosystem, i.e. (i) a shallow lake
658 colonized by large sedge mats during the rainy season and (ii) a waterlogged marsh-like regime at the
659 end of the dry season due to high evaporation rates (Delalande et al., 2008a, 2008b).

660 The period that corresponds to unit III at Kyambangunguru starts with relatively warm mean annual air
661 temperatures, at ca. 22 °C, followed by an abrupt cooling to 20 °C at ca. 0.5 ka cal. BP (Fig. 8). A similar
662 abrupt event was also identified at Lake Tanganyika (Tierney et al., 2010a; Fig. 8), in the Ethiopian
663 Highlands and in southern Africa (Nicholson et al., 2013 and references therein) and could coincide
664 with the transition between a "Medieval Climate Anomaly" (MCA; based on Jones et al. (2001) time
665 boundaries: ca. 1.0 – 0.8 ka cal. BP) and a Little Ice Age (LIA; 0.7 – 0.1 ka cal. BP; Matthews and
666 Briffa, 2005) in the African continent. The occurrence of climatic shifts in Africa that could be related
667 to the European MCA and LIA events is currently under debate but a growing body of research seems
668 to support such a cross-latitude connection (e.g. Lüning et al., 2018; Russell and Johnson, 2007; Tierney
669 et al., 2013). At Kyambangunguru, the last 500 yrs exhibit the coldest temperatures of the record which
670 would support the existence of a "Little Ice Age" equivalent in East Africa, in agreement with records
671 from nearby Lake Malawi (Branchu et al., 2010; Powers et al., 2011; Fig. 8). At the transition between
672 units II and III (ca. 1.4 – 0.8 ka cal. BP) the δ^2H_{wax} values decrease, consistent with the reestablishment
673 of higher P/E ratio under wetter conditions and the spreading of Proteaceae and the recovery of the
674 *Uapaca* woodlands, as observed in the pollen record. At 0.8 ka cal. BP, the canopy density started to
675 decrease, the fire activity increased, which led to a spread in the grassland communities, maintained
676 until nowadays. Similar conditions were recorded at Lake Masoko (Vincens et al., 2003). Intensification
677 of human activity in the region could be responsible for such vegetation changes, especially as no shift
678 is observed in the δ^2H_{wax} values during this period. Additional high-resolution reconstructions in the
679 RVP and the neighbouring provinces are necessary to better assess the relative contribution of human
680 versus climatic nature of these recent environmental shifts.

681

682 5.2. Implications for climate dynamics in East Africa during the late Holocene and its impact on
683 highland wetland ecology

684 The temperature and P/E ratio records at Kyambangunguru show a high variability over the last 4.0 ka
685 cal. BP. The main two warm periods, before ca. 3.7 ka cal. BP and between ca. 2.2 and 1.0 ka cal. BP,
686 were generally accompanied by drier conditions (Figs. 8 and 9). A major dry event at 4.2 ka cal. BP is

687 a common feature in many tropical and temperate records and was interpreted as a southward migration
688 of the ITCZ (e.g. Gasse, 2000; Mayewski et al., 2004). A severe drought has also been observed in many
689 other East African sites around 2.0 ka cal. BP (Marchant et al., 2018) and could have been related to the
690 dry and warm period centred at ca. 1.5 ka cal. BP at Kyambangunguru. The discrepancy in timing
691 between the RVP and the other tropical East African records may be related to the unique location of
692 the RVP at the southern end of the tropical climatic belt (≈ 10 °S), i.e. at the transition between two
693 hydro-climatic regimes (the north-eastern and the southern ones). Two cold and wet periods were
694 identified, between ca. 3.3 and 2.0 ka cal. BP and since ca. 0.6 ka cal. BP. The latter period is concurrent
695 with the European Little Ice Age and suggests that this cold event may have occurred globally (e.g.
696 Brown and Johnson, 2005). The warm and dry period at ca. 1.5 ka cal. BP and the two cold and wet
697 events all correspond to cold periods identified by Wanner et al. (2011) supporting the idea that the
698 Holocene climatic variability is at least partly driven by global scale events (e.g. solar and volcanic
699 activities, changes in the thermohaline circulation). However, it emphasizes that these processes seemed
700 to have contrasting effects at different latitudes (cooling vs. warming).

701 A major ecological shift that led to the transition from a shallow lake to a peatland at Kyambangunguru
702 started at ca. 2.5 ka cal. BP, in a rather wet environment, 300 years before the δ^2H_{wax} exhibit an abrupt
703 shift towards drier conditions (Fig 9). This time offset suggests that the ecological change recorded at
704 Kyambangunguru was primarily due to a hydroseral succession, i.e. the natural progressive colonisation
705 and infilling of a freshwater lake by different types of macrophytes leading to its transition to a swamp
706 which could eventually turn into a forest (Charman, 2002). A drier peatland was established at ca. 2.2
707 ka cal. BP and sustained until ca. 1.4 ka cal. BP likely as a result of combined warm and dry conditions,
708 which significantly lowered the P/E ratio of the wetland (Fig. 8 and 9). This is consistent with the abrupt
709 change at ca. 2.2 ka cal. BP observed in the biotic communities: planktonic and *Nymphaea* communities
710 disappeared, while *Cyperus* spp. took over in only a century (Fig. 6). This behaviour suggests a threshold
711 effect, which may reflect an autogenic hydroseral development triggered by gradual warming
712 conditions. Previous studies have shown the ability of *Nymphaea* spp. to form mats floating at the
713 surface of the water (Charman, 2002; Ellery et al., 1990) and pointed it out as a common step in the
714 hydroseral succession leading to the conversion of a freshwater body to a swamp (Kratz and DeWitt,

715 1986; Swan and Gill, 1970). The development of floating mats could be accelerated in the tropics, as
716 the warm air temperatures hold up high vegetation productivity rates (Talling et al., 1998). The slight
717 warming recorded at ca. 2.6 ka cal. BP (by the br GDGTs; Fig. 8) could then have acted as a positive
718 feedback in promoting high rates of vegetation productivity. The consequences of this fast development
719 of floating mats are (i) large inputs of OM in the sediment, which progressively infilled the lake, (ii) a
720 vertical expansion of the mats by peat accumulation, and (iii) a horizontal expansion and partial covering
721 of the surface of the lake. From ca. 3.3 to 2.3 ka cal. BP (Fig. 6), opposite trends are observed in the
722 distribution of plankton and *Nymphaea* suggesting that the more *Nymphaea* mats would cover the lake
723 surface, the less light would penetrate the water column leading to a decrease in microalgae abundance,
724 supporting the proposed mechanism of lake infilling.

725 This terrestrialization process was interrupted at ca. 1.4 ka cal. BP, when pronounced fluctuations in the
726 water table are revealed by the presence of *Enthorriza* in the microfossil record (ca. 1.4 – 0.7 ka cal. BP;
727 Fig. 6). The water balance, recorded by the δ^2H_{wax}, increased over this period, suggesting a relative
728 increase in precipitation (Fig. 9) in agreement with the spread of Proteaceae and *Uapaca* in the terrestrial
729 pollen. This likely re-flooded the marsh and created patches of open water, where phytoplankton, and
730 then *Nymphaea*, could re-colonise the marsh (Fig. 6). A similar ecosystem change was encountered at
731 the same period in a mountainous marsh in Madagascar (Bourdon et al., 2000). This period of water
732 fluctuations, synchronous with the Medieval Climate Anomaly (MCA; 1.0 – 0.8 ka cal. BP), is the only
733 period of the investigating 4000 yr record when conditions were warm and wet at Kyambangunguru,
734 suggesting that its origin may be different from the other recorded climatic changes. The MCA is
735 described as warm and dry in most north-eastern Africa (Lüning et al., 2017; Nash et al., 2016;
736 Nicholson et al., 2013) and humid in southern Africa (e.g. Nash et al., 2016; Tyson and Lindesay, 1992;
737 Woodborne et al., 2015). A recent literature review by Lüning et al. (2018) suggests a transition zone
738 across Tanzania with increased signs of humidity along a NE-SW transect. Notably, Buckles et al.
739 (2016) and Finch et al. (2017) recorded wet conditions at Lake Challa until ca. 800 BP and at the
740 Kwasebuge peat bog until ca. 675 BP, respectively. Hence the Kyambangunguru record presented here
741 extends this transitional zone to the southeast, in agreement with the hydroclimatic interpretation of a
742 biogenic silica record by Johnson et al. (2004) at Lake Malawi.

6. Conclusions

The detailed multi-proxy analysis of a 4-m peat core covering the late Holocene (4000 years) reveals rapid and profound ecological changes of the Kyambangunguru wetland in the Rungwe Volcanic Province (RVP), southwestern Tanzania. Around 2.2 ka cal. BP, a shallow crater lake turned into a peatland. Starting at ca. 0.9 ka cal. BP the water level in the marsh increased, creating a shallow lake during the rainy season and a peaty marsh during the dry season. These significant ecological fluctuations correlated with major changes of the Late Holocene East African climate. Notably, the air temperatures remained high and the reconstructed precipitation low between ca. 2.2 and 0.9 ka cal. BP, which allowed the peatland terrestrialization to sustain. This study represents the first detailed late Holocene quantitative air temperature reconstruction from the RVP region. We identified a succession of cold/warm/cold events, largely in phase with the other regional East African climate records and with the cold periods identified worldwide by Wanner et al. (2011). This further supports that global scale processes may be the main drivers of the Holocene climatic variability. Moreover, warm conditions during the MCA followed by abrupt cooling during the LIA were observed at Kyambangunguru and elsewhere in East Africa suggesting that these two recent events occurred globally. The precipitation pattern at Kyambangunguru during these two events is opposite to most of the more north-eastern African records and rather resembles the southern African climatic records. Recent additional precipitation records in Tanzania also show such a pattern. Tanzania seemed thus to be located at the transition zone between two hydro-climatic poles (north-eastern and southern Africa) and to have experienced a variable relative contribution of these two poles over the last millennium. This study further demonstrates that peatlands and marshes provide valuable, high resolution climatic archives in the tropics that offer novel avenues of research for understanding linkages between the Holocene climate variability and ecosystem change in the tropics.

Acknowledgments:

The authors warmly thank the RESON (Rungwe Environmental Science Observatory Network) and those who helped during field trips, notably Stephen Kajula, Winne Mosena, Matokeo Arbogast, Stephen Warui, Marcel Hale and the inhabitants of Masoko. Paul Donohoe and Bernard Bowler are acknowledged for their technical support at Newcastle University. A special thank is given to Patrick Coyac for his graphical help and to Peguy for providing essential writing tool. ^{14}C dating was performed at the ARTEMIS platform, funded by the INSU (CNRS, France). Pollen and NPPs were analysed by Piotr Kołaczek and Monika Karpińska-Kołaczek respectively and the plant macrofossils by Mariusz Gałka. This work was supported by the EC2CO program (CNRS/INSU, France, P.I. A. Huguet), the UPMC (PhD scholarship to S. Coffinet) and the European Association of Organic Geochemistry (EAOG) via a travel grant awarded to S. Coffinet.

Figure and Table captions:

Figure 1: Regional setting and climatic conditions of the studied site. A: geographical location of the Rungwe Volcanic Province (RVP, adapted from Delalande, 2008), the green lines outline the maximal positions of the intertropical convergence zone (ITCZ) over the year, the blue lines delimitate the equatorial rain region and the histograms show the monthly mean precipitation values (mm) at the main East African weather stations; B: topographical map of the RVP and location of the Kyambangunguru marsh; C: lake level (black dots), precipitation (blue bars) and marsh water δ^2H composition (red dots) variations over one calendar year; D-E: pictures of the Kyambangunguru crater marsh taken in July 2014.

Figure 2: Lithology (A) and Bayesian age-depth model (B). The A values indicate the agreement between the modelled and the calibrated age and the A_{model} the agreement of the model itself. TOM samples are in black, wood samples in red and tephra ones in grey. Horizontal dotted lines represent the model boundaries (see text for details) and excluded dates are identified as outliers.

Figure 3: Quantitative palynofacies: relative abundance of the main organic aggregates analysed by photonic microscopy in transmitted light. In green: ligno-cellulosic tissues (LC): (i) fresh LC detected as translucent LC (tLC) in light green, (ii) slightly degraded/amorphised LC (saLC) in yellow-green and (iii) totally degraded/amorphous LC, characterised by red aggregates of amorphous OM (rAOM) in dark green. In orange: mycelium (myc) fragments. In blue: planktonic remains (algOM).

Figure 4: Plant macro-fossil diagram. Results are given in absolute numbers. For the legend of the lithology column see Fig. 2. Roman numbers indicate the three ecological units as defined in the discussion part.

Figure 5: Woodland pollen diagram for the Kyambangunguru marsh showing relative percentages of the selected taxa. The grey pattern shows a 10x magnification. For the legend of the lithology column see Fig. 2. Roman numbers indicate the three ecological units as defined in the discussion part.

Figure 6: Ferns, aquatic pollen and NPP diagram for the Kyambangunguru marsh showing relative percentages of the selected taxa. The grey pattern shows a 10x magnification. For the legend of the lithology column see Fig. 2. Roman numbers indicate the three ecological units as defined in the discussion part.

Figure 7: Lithology (A; see details in Fig. 2), total organic carbon over total nitrogen atomic ratio (B), br GDGT-derived pH (C; based on Tierney et al. (2010b) calibration) and *n*-alkane distribution indices (D-E; ACL and Paq, respectively). The three units discussed in the text are also represented along with their ecological interpretation.

Figure 8: (a) Lake Tanganyika TEX_{86}-derived lake surface temperature (LST) of the last 4000 (black contour red dots) and 1500 (red plain dots) years (Tierney et al., 2010a and 2008 respectively) and (b) Lake Malawi TEX_{86}-derived LST of the last 4000 (black contour yellow dots) and 700 (yellow plain dots) years (Powers et al., 2005, 2011) compared to (c) Kyambangunguru br GDGT-derived MAAT (present study). The three units described in the text are also represented (dashed lines).

Figure 9: (a) Lake Edward Mg (mol %; Russell and Johnson, 2005) and (b) Kyambangunguru δ^2Hwax records for the last 4000 years (present study). The three units described in the text are also represented (dashed lines).

Table 1: AMS Radiocarbon chronology of the core KYAM12 (2012). Calibrated median age and range (2σ) were obtained using OxCal 4.3 software (Bronk Ramsey and Lee, 2013) with the ShCal 13 atmospheric curve (Hogg et al., 2013) and Bomb13SH3 (Hua et al., 2013).

References:

Alin, S.R., Cohen, A.S., 2003. Lake-level history of Lake Tanganyika, East Africa, for the past 2500 years based on ostracode-inferred water-depth reconstruction. Palaeogeogr. Palaeoclimatol. Palaeoecol. 199, 31–49. https://doi.org/10.1016/S0031-0182(03)00484-X

Amesbury, M.J., Barber, K.E., Hughes, P.D.M., 2012. Can rapidly accumulating Holocene peat profiles provide sub-decadal resolution proxy climate data? J. Quat. Sci. 27, 757–770. https://doi.org/10.1002/jqs.2561

Basalirwa, C. p. k., Odiyo, J. o., Mngodo, R. j., Mpeta, E. j., 1999. The climatological regions of Tanzania based on the rainfall characteristics. Int. J. Climatol. 19, 69–80. https://doi.org/10.1002/(SICI)1097-0088(199901)19:1<69::AID-JOC343>3.0.CO;2-M

Berglund, B.E., Ralska-Jasiewiczowa, M., 1986. Handbook of Holocene Palaeoecology and Palaeohydrology, J. Wiley & Sons Ltd. ed. Berglund, B.E., Ralska- Jasiewiczowa, M., Chichester-Toronto.

Berke, M.A., Johnson, T.C., Werne, J.P., Schouten, S., Sinninghe Damsté, J.S., 2012. A mid-Holocene thermal maximum at the end of the African Humid Period. Earth Planet. Sci. Lett. 351, 95–104. https://doi.org/10.1016/j.epsl.2012.07.008

Blackford, J., 2000. Palaeoclimatic records from peat bogs. Trends Ecol. Evol. 15, 193–198. https://doi.org/10.1016/S0169-5347(00)01826-7

Bonnefille, R., Roeland, J.C., Guiot, J., 1990. Temperature and rainfall estimates for the past 40,000 years in equatorial Africa. Nature 346, 347. https://doi.org/10.1038/346347a0

Bourdon, S., Laggoun-Défarge, F., Disnar, J.-R., Maman, O., Guillet, B., Derenne, S., Largeau, C., 2000. Organic matter sources and early diagenetic degradation in a tropical peaty marsh (Tritrivakely, Madagascar). Implications for environmental reconstruction during the Sub-Atlantic. Org. Geochem. 31, 421–438.

Boussafir, M., Sifeddine, A., Jacob, J., Foudi, M., Cordeiro, R.C., Albuquerque, A.L.S., Abrao, J.J., Turcq, B., 2012. Petrographical and geochemical study of modern lacustrine sedimentary organic matter (Lagoa do Caçò, Maranão, Brazil): Relationship between early diagenesis, organic sedimentation and lacustrine filling. Org. Geochem. 47, 88–98. https://doi.org/10.1016/j.orggeochem.2012.03.013

Branchu, P., Bergonzini, L., Delvaux, D., De Batist, M., Golubev, V., Benedetti, M., Klerkx, J., 2005. Tectonic, climatic and hydrothermal control on sedimentation and water chemistry of northern Lake Malawi (Nyasa), Tanzania. J. Afr. Earth Sci. 43, 433–446. https://doi.org/10.1016/j.jafrearsci.2005.09.004

Branchu, P., Bergonzini, L., Pons-Branchu, E., Violier, E., Dittrich, M., Massault, M., Ghaleb, B., 2010. Lake Malawi sediment and pore water chemistry: Proposition of a conceptual model for stratification intensification since the end of the Little Ice Age.

Glob. Planet. Change, Quaternary and Global Change: Review and Issues Special issue in memory of Hugues FAURE 72, 321–330. https://doi.org/10.1016/j.gloplacha.2010.01.008

Bray, E.E., Evans, E.D., 1961. Distribution of *n*-paraffins as a clue to recognition of source beds. Geochim. Cosmochim. Acta 22, 2–15. https://doi.org/10.1016/0016-7037(61)90069-2

Bronk Ramsey, C.B., 1995. Radiocarbon calibration and analysis of stratigraphy: The OxCal program. Radiocarbon 37, 425–430. https://doi.org/10.1017/S0033822200030903

Bronk Ramsey, C.B., 2008. Deposition models for chronological records. Quat. Sci. Rev., INTegration of Ice-core, Marine and Terrestrial records (INTIMATE): Refining the record of the Last Glacial-Interglacial Transition 27, 42–60. https://doi.org/10.1016/j.quascirev.2007.01.019

Bronk Ramsey, C.B., 2009. Bayesian analysis of radiocarbon dates. Radiocarbon 51, 337–360. https://doi.org/10.1017/S0033822200033865

Bronk Ramsey, C.B., Lee, S., 2013. Recent and planned developments of the program OxCal. Radiocarbon 55, 720–730. https://doi.org/10.1017/S0033822200057878

Brown, E.T., Johnson, T.C., 2005. Coherence between tropical East African and South American records of the Little Ice Age. Geochem. Geophys. Geosystems 6, Q12005. https://doi.org/10.1029/2005GC000959

Buckles, L.K., Verschuren, D., Weijers, J.W.H., Cocquyt, C., Blaauw, M., Sinninghe Damsté, J.S., 2016. Interannual and (multi-)decadal variability in the sedimentary BIT index of Lake Challa, East Africa, over the past 2200 years: assessment of the precipitation proxy. Clim Past 12, 1243–1262. https://doi.org/10.5194/cp-12-1243-2016

Chambers, F.M., Booth, R.K., De Vleeschouwer, F., Lamentowicz, M., Le Roux, G., Mauquoy, D., Nichols, J.E., van Geel, B., 2012. Development and refinement of proxy-climate indicators from peats. Quat. Int., Peat Stratigraphy and Climate Change 268, 21–33. https://doi.org/10.1016/j.quaint.2011.04.039

Charman, D., 2002. Peatlands and Environmental Change, John Wiley & Sons. ed. England.

Coffinet, S., Huguet, A., Williamson, D., Bergonzini, L., Anquetil, C., Majule, A., Derenne, S., 2015. Occurrence and distribution of glycerol dialkanol diethers and glycerol dialkyl glycerol tetraethers in a peat core from SW Tanzania. Org. Geochem. 83–84, 170–177. https://doi.org/10.1016/j.orggeochem.2015.03.013

Coffinet, S., Huguet, A., Pedentchouk, N., Bergonzini, L., Omuombo, C., Williamson, D., Anquetil, C., Jones, M., Majule, A., Wagner, T., Derenne, S., 2017. Evaluation of branched GDGTs and leaf wax n-alkane δ2H as (paleo) environmental proxies in East Africa. Geochim. Cosmochim. Acta 198, 182–193. https://doi.org/10.1016/j.gca.2016.11.020

Cottereau, E., Arnold, M., Moreau, C., Baqué, D., Bavay, D., Caffy, I., Comby, C., Dumoulin, J.-P., Hain, S., Perron, M., Salomon, J., Setti, V., 2007. Artemis, the new ^{14}C AMS at LMC14 in Saclay, France. Radiocarbon 49, 291–299. https://doi.org/10.1017/S0033822200042211

Davis, M.B., Deevey Jr., E.S., 1964. Pollen accumulation rates: estimates from late-glacial sediment of Rogers Lake. Science 145, 1293–1295.

Delalande, M., 2008. Hydrologie et géochimie isotopique du lac Masoko et de lacs volcaniques de la province active du Rungwe (Sud-Ouest Tanzanie). Université Paris Sud-Paris XI.

Delalande, M., Bergonzini, L., Branchu, P., Filly, A., Williamson, D., 2008a. Hydroclimatic and geothermal controls on the salinity of Mbaka Lakes (SW Tanzania): Limnological and paleolimnological implications. J. Hydrol. 359, 274–286. https://doi.org/10.1016/j.jhydrol.2008.07.007

Delalande, M., Bergonzini, L., Massault, M., 2008b. Mbaka lakes isotopic (18O and 2H) and water balances: discussion on the used atmospheric moisture compositions. Isotopes Environ. Health Stud. 44, 71–82. https://doi.org/10.1080/10256010801887414

Eglinton, G., Hamilton, R.J., 1967. Leaf epicuticular waxes. Science, New Series 156, 1322–1335.

Ellery, K., Ellery, W.N., Rogers, K.H., Walker, B.H., 1990. Formation, colonization and fate of floating sudds in the Maunachira river system of the Okavango Delta, Botswana. Aquat. Bot. 38, 315–329. https://doi.org/10.1016/0304-3770(90)90027-I

Estep, M., Hoering, T., 1980. Biogeochemistry of the stable hydrogen isotopes. Geochim. Cosmochim. Acta 44, 1197–1206. https://doi.org/10.1016/0016-7037(80)90073-3

Ficken, K.J., Li, B., Swain, D.L., Eglinton, G., 2000. An *n*-alkane proxy for the sedimentary input of submerged/floating freshwater aquatic macrophytes. Org. Geochem. 31, 745–749. https://doi.org/10.1016/S0146-6380(00)00081-4

Filippi, M.L., Talbot, M.R., 2005. The palaeolimnology of northern Lake Malawi over the last 25 ka based upon the elemental and stable isotopic composition of sedimentary organic matter. Quat. Sci. Rev. 24, 1303–1328. https://doi.org/10.1016/j.quascirev.2004.10.009

Finch, J., Marchant, R., Courtney Mustaphi, C.J., 2017. Ecosystem change in the South Pare Mountain bloc, Eastern Arc Mountains of Tanzania. The Holocene 27, 796–810. https://doi.org/10.1177/0959683616675937

Finsinger, W., Tinner, W., 2005. Minimum count sums for charcoal concentration estimates in pollen slides: accuracy and potential errors. The Holocene 15, 293–297.

Fontijn, K., Ernst, G.G.J., Elburg, M.A., Williamson, D., Abdallah, E., Kwelwa, S., Mbede, E., Jacobs, P., 2010. Holocene explosive eruptions in the Rungwe Volcanic Province, Tanzania. J. Volcanol. Geotherm. Res. 196, 91–110. https://doi.org/10.1016/j.jvolgeores.2010.07.021

Fontijn, K., Williamson, D., Mbede, E., Ernst, G.G.J., 2012. The Rungwe Volcanic Province, Tanzania – A volcanological review. J. Afr. Earth Sci. 63, 12–31. https://doi.org/10.1016/j.jafrearsci.2011.11.005

Gałka, M., Bergonzini, L., Williamson, D., Majule, A., Masao, C., Huguet, A., 2015. Macrofossil evidence of Late Holocene presence of Aldrovanda vesiculosa L. in Central-Eastern Europe (Poland) and East Africa (Tanzania). Quat. Int., Palaeolandscapes from Saalian to Weichselian: INQUA TERPRO Commission, Peribaltic International Field Symposium, Lithuania 386, 186–190. https://doi.org/10.1016/j.quaint.2015.05.058

Garcin, Y., Williamson, D., Taieb, M., Vincens, A., Mathé, P.-E., Majule, A., 2006. Centennial to millennial changes in maar-lake deposition during the last 45,000 years in tropical Southern Africa (Lake Masoko, Tanzania). Palaeogeogr. Palaeoclimatol. Palaeoecol. 239, 334–354. https://doi.org/10.1016/j.palaeo.2006.02.002

Garcin, Y., Williamson, D., Bergonzini, L., Radakovitch, O., Vincens, A., Buchet, G., Guiot, J., Brewer, S., Mathé, P.-E., Majule, A., 2007. Solar and anthropogenic imprints on Lake Masoko (southern Tanzania) during the last 500 years. J. Paleolimnol. 37, 475–490. https://doi.org/10.1007/s10933-006-9033-6

Gasse, F., 2000. Hydrological changes in the African tropics since the Last Glacial Maximum. Quat. Sci. Rev. 19, 189–211. https://doi.org/10.1016/S0277-3791(99)00061-X

Gelorini, V., Verbeken, A., van Geel, B., Cocquyt, C., Verschuren, D., 2011. Modern non-pollen palynomorphs from East African lake sediments. Rev. Palaeobot. Palynol. 164, 143–173. https://doi.org/10.1016/j.revpalbo.2010.12.002

Gibert, E., Bergonzini, L., Massault, M., Williamson, D., 2002. AMS-^{14}C chronology of 40.0 cal ka BP continuous deposits from a crater lake (Lake Massoko, Tanzania): Modern

961 water balance and environmental implications. Palaeogeogr. Palaeoclimatol.
962 Palaeoecol. 187, 307–322. https://doi.org/10.1016/S0031-0182(02)00483-2
963 Gonfiantini, R., 1986. Chapter 3 - Environmental isotopes in lake studies, in: Fritz, P., Fontes,
964 J.C. (Eds.), The Terrestrial Environment, B, Handbook of Environmental Isotope
965 Geochemistry. Elsevier, Amsterdam, pp. 113–168. https://doi.org/10.1016/B978-0-
966 444-42225-5.50008-5
967 Gosling, W.D., Miller, C.S., Livingstone, D.A., 2013. Atlas of the tropical West African
968 pollen flora. Rev. Palaeobot. Palynol. Palynology of tropical Africa 199, 1–135.
969 https://doi.org/10.1016/j.revpalbo.2013.01.003
970 Graz, Y., Di-Giovanni, C., Copard, Y., Laggoun-Défarge, F., Boussafir, M., Lallier-Vergès,
971 E., Baillif, P., Perdereau, L., Simonneau, A., 2010. Quantitative palynofacies analysis
972 as a new tool to study transfers of fossil organic matter in recent terrestrial
973 environments. Int. J. Coal Geol. 84, 49–62. https://doi.org/10.1016/j.coal.2010.08.006
974 Gupta, A.K., Beentje, H.J., 2017. Caldesia parnassifolia. The IUCN Red List of Threatened
975 Species 2017: e.T162381A83996588.
976 Han, D., Ha, H.K., Hwang, C.Y., Lee, B.Y., Hur, H.-G., Lee, Y.K., 1968. Bacterial
977 distribution along stratified water Columns in the pacific sector of the Arctic ocean.
978 Deep Sea Res. Part II Top. Stud. Oceanogr. https://doi.org/10.1016/j.dsr2.2014.06.007
979 Hogg, A.G., Hua, Q., Blackwell, P.G., Niu, M., Buck, C.E., Guilderson, T.P., Heaton, T.J.,
980 Palmer, J.G., Reimer, P.J., Reimer, R.W., Turney, C.S.M., Zimmerman, S.R.H., 2013.
981 SHCal13 Southern Hemisphere Calibration, 0–50,000 Years cal BP. Radiocarbon 55,
982 1889–1903. https://doi.org/10.2458/azu_js_rc.55.16783
983 Hua, Q., Barbetti, M., Rakowski, A.Z., 2013. Atmospheric radiocarbon for the period 1950–
984 2010. Radiocarbon 55, 2059–2072. https://doi.org/10.2458/azu_js_rc.v55i2.16177
985 Johnson, T.C., Brown, E.T., McManus, J., 2004. Diatom productivity in northern Lake
986 Malawi during the past 25,000 years: Implications for the position of the intertropical
987 convergence zone at millennial and shorter time scales, in: Battarbee, R.W., Gasse, F.,
988 Stickley, C.E. (Eds.), Past climate variability through Europe and Africa. Springer,
989 Dordrecht, pp. 93–116.
990 Jones, P.D., Osborn, T.J., Briffa, K.R., 2001. The evolution of climate over the last
991 Millennium. Science 292, 662–667. https://doi.org/10.1126/science.1059126
992 Killops, V., Killops, S., 2005. Introduction to organic geochemistry 2d edition. Blackwel
993 Publishing Ltd.
994 Konecky, B., Russell, J., Huang, Y., Vuille, M., Cohen, L., Street-Perrott, F.A., 2014. Impact
995 of monsoons, temperature, and CO_2 on the rainfall and ecosystems of Mt. Kenya
996 during the Common Era. Palaeogeogr. Palaeoclimatol. Palaeoecol. 396, 17–25.
997 https://doi.org/10.1016/j.palaeo.2013.12.037
998 Kratz, T.K., DeWitt, C.B., 1986. Internal factors controlling peatland-lake ecosystem
999 development. Ecology 67, 100–107. https://doi.org/10.2307/1938507
1000 Laggoun-Défarge, F., Mitchell, E., Gilbert, D., Disnar, J.-R., Comont, L., Warner, B.G.,
1001 Buttler, A., 2008a. Cut-over peatland regeneration assessment using organic matter
1002 and microbial indicators (bacteria and testate amoebae). J. Appl. Ecol. 45, 716–727.
1003 Laggoun-Défarge, F., Gilbert, D., Buttler, A., Epron, D., Francez, A.-J., Grasset, L., Mitchell,
1004 E.A.D., Guimbaud, C., Roy, J.-C., 2008b. Effects of experimental warming on carbon
1005 sink function of a temperate pristine mire : the PEATWARM project. in: International
1006 Peat Society Congress. Tullamore, Irlande.
1007 Loisel, J., Yu, Z., 2013. Surface vegetation patterning controls carbon accumulation in
1008 peatlands. Geophys. Res. Lett. 40, 5508–5513. https://doi.org/10.1002/grl.50744
1009 Loomis, S.E., Russell, J.M., Ladd, B., Street-Perrott, F.A., Sinninghe Damsté, J.S., 2012.
1010 Calibration and application of the branched GDGT temperature proxy on East African

lake sediments. Earth Planet. Sci. Lett. 357–358, 277–288. https://doi.org/10.1016/j.epsl.2012.09.031
Loomis, S.E., Russell, J.M., Lamb, H.F., 2015. Northeast African temperature variability since the Late Pleistocene. Palaeogeogr. Palaeoclimatol. Palaeoecol. 423, 80–90. https://doi.org/10.1016/j.palaeo.2015.02.005
Lüning, S., Gałka, M., Vahrenholt, F., 2017. Warming and cooling: the medieval climate anomaly in Africa and Arabia. Paleoceanography 32, 2017PA003237. https://doi.org/10.1002/2017PA003237
Lüning, S., Gałka, M., Danladi, I.B., Adagunodo, T.A., Vahrenholt, F., 2018. Hydroclimate in Africa during the Medieval Climate Anomaly. Palaeogeogr. Palaeoclimatol. Palaeoecol. 495, 309–322. https://doi.org/10.1016/j.palaeo.2018.01.025
Majule, A.E., 2010. The impact of land management practices on soil quality and implications on smallholder productivity. Environ. Econ. 1, 59–67.
Marchant, R., Taylor, D., 1998. Dynamics of montane forest in central Africa during the late Holocene: a pollen-based record from western Uganda. The Holocene 8, 375–381. https://doi.org/10.1191/095968398672993971
Marchant, R., Richer, S., Boles, O., Capitani, C., Courtney-Mustaphi, C.J., Lane, P., Prendergast, M.E., Stump, D., De Cort, G., Kaplan, J.O., Phelps, L., Kay, A., Olago, D., Petek, N., Platts, P.J., Punwong, P., Widgren, M., Wynne-Jones, S., Ferro-Vázquez, C., Benard, J., Boivin, N., Crowther, A., Cuní-Sanchez, A., Deere, N.J., Ekblom, A., Farmer, J., Finch, J., Fuller, D., Gaillard-Lemdahl, M.-J., Gillson, L., Githumbi, E., Kabora, T., Kariuki, R., Kinyanjui, R., Kyazike, E., Lang, C., Lejju, J., Morrison, K.D., Muiruri, V., Mumbi, C., Muthoni, R., Muzuka, A., Ndiema, E., Kabonyi Nzabandora, C., Onjala, I., Schrijver, A.P., Rucina, S., Shoemaker, A., Thornton-Barnett, S., van der Plas, G., Watson, E.E., Williamson, D., Wright, D., 2018. Drivers and trajectories of land cover change in East Africa: Human and environmental interactions from 6000 years ago to present. Earth-Sci. Rev. 178, 322–378. https://doi.org/10.1016/j.earscirev.2017.12.010
Matthews, J.A., Briffa, K.R., 2005. The 'little Ice Age': Re-evaluation of an evolving concept. Geogr. Ann. Ser. Phys. Geogr. 87, 17–36. https://doi.org/10.1111/j.0435-3676.2005.00242.x
Mayewski, P.A., Rohling, E.E., Curt Stager, J., Karlén, W., Maasch, K.A., David Meeker, L., Meyerson, E.A., Gasse, F., van Kreveld, S., Holmgren, K., Lee-Thorp, J., Rosqvist, G., Rack, F., Staubwasser, M., Schneider, R.R., Steig, E.J., 2004. Holocene climate variability. Quat. Res. 62, 243–255. https://doi.org/10.1016/j.yqres.2004.07.001
Meyers, P.A., 1997. Organic geochemical proxies of paleoceanographic, paleolimnologic, and paleoclimatic processes. Org. Geochem. 27, 213–250. https://doi.org/10.1016/S0146-6380(97)00049-1
Miola, A., 2012. Tools for Non-Pollen Palynomorphs (NPPs) analysis: A list of Quaternary NPP types and reference literature in English language (1972–2011). Rev. Palaeobot. Palynol., Non-pollen Palynomorphs as Relevant indicators in Palaeoecology and Archaeobotany 186, 142–161. https://doi.org/10.1016/j.revpalbo.2012.06.010
Morris, P.J., Baird, A.J., Young, D.M., Swindles, G.T., 2015. Untangling climate signals from autogenic changes in long-term peatland development. Geophys. Res. Lett. 42, 2015GL066824. https://doi.org/10.1002/2015GL066824
Nalepka, D., Walanus, A., 2003. Data processing in pollen analysis. Acta Palaeobot. 43, 125–134.
Nash, D.J., De Cort, G., Chase, B.M., Verschuren, D., Nicholson, S.E., Shanahan, T.M., Asrat, A., Lézine, A.-M., Grab, S.W., 2016. African hydroclimatic variability during the last 2000 years. Quat. Sci. Rev. 154, 1–22. https://doi.org/10.1016/j.quascirev.2016.10.012

Nichols, J.E., Peteet, D.M., Moy, C.M., Castañeda, I.S., McGeachy, A., Perez, M., 2014. Impacts of climate and vegetation change on carbon accumulation in a south-central Alaskan peatland assessed with novel organic geochemical techniques. The Holocene 24, 1146–1155. https://doi.org/10.1177/0959683614540729

Nicholson, S.E., Nash, D.J., Chase, B.M., Grab, S.W., Shanahan, T.M., Verschuren, D., Asrat, A., Lézine, A.-M., Umer, M., 2013. Temperature variability over Africa during the last 2000 years. The Holocene 23, 1085–1094. https://doi.org/10.1177/0959683613483618

Nivet, F., Bergonzini, L., Mathé, P.-E., Noret, A., Monvoisin, G., Majule, A., Williamson, D., 2018. Influence of the balance of the Intertropical Front on seasonal variations of rainfall isotopic compositions at Kisiba Masoko (Rungwe Volcanic Province, SW, Tanzania). Isotopes Environ. Health Stud.

Page, S.E., Rieley, J.O., Banks, C.J., 2011. Global and regional importance of the tropical peatland carbon pool. Glob. Change Biol. 17, 798–818. https://doi.org/10.1111/j.1365-2486.2010.02279.x

Peterse, F., Prins, M.A., Beets, C.J., Troelstra, S.R., Zheng, H., Gu, Z., Schouten, S., Damsté, J.S.S., 2011. Decoupled warming and monsoon precipitation in East Asia over the last deglaciation. Earth Planet. Sci. Lett. 301, 256–264. https://doi.org/10.1016/j.epsl.2010.11.010

Powers, L.A., Johnson, T.C., Werne, J.P., Castanada, I.S., Hopmans, E.C., Damste, J.S.S., Schouten, S., 2005. Large temperature variability in the southern African tropics since the Last Glacial Maximum. Geophys. Res. Lett. 32. https://doi.org/10.1029/2004GL022014

Powers, L.A., Johnson, T.C., Werne, J.P., Castañeda, I.S., Hopmans, E.C., Sinninghe Damsté, J.S., Schouten, S., 2011. Organic geochemical records of environmental variability in Lake Malawi during the last 700 years, Part I: The TEX86 temperature record. Palaeogeogr. Palaeoclimatol. Palaeoecol., Southern hemisphere tropical climate over the past 145ka: Results of the Lake Malawi Scientific Drilling Project, East Africa 303, 133–139. https://doi.org/10.1016/j.palaeo.2010.09.006

Riess, K., Bauer, R., Kellner, R., Kemler, M., Piątek, M., Vánky, K., Begerow, D., 2015. Identification of a new order of root-colonising fungi in the Entorrhizomycota: Talbotiomycetales ord. nov. on eudicotyledons. IMA Fungus 6, 129–133. https://doi.org/10.5598/imafungus.2015.06.01.07

Rucina, S.M., Muiruri, V.M., Downton, L., Marchant, R., 2010. Late-Holocene savanna dynamics in the Amboseli Basin, Kenya. The Holocene 20, 667–677. https://doi.org/10.1177/0959683609358910

Russell, J.M., Johnson, T.C., Talbot, M.R., 2003. A 725 yr cycle in the climate of central Africa during the late Holocene. Geology 31, 677–680. https://doi.org/10.1130/G19449.1

Russell, J.M., Johnson, T.C., 2005. A high-resolution geochemical record from Lake Edward, Uganda Congo and the timing and causes of tropical African drought during the late Holocene. Quat. Sci. Rev. 24, 1375–1389. https://doi.org/10.1016/j.quascirev.2004.10.003

Russell, J.M., Johnson, T.C., 2007. Little Ice Age drought in equatorial Africa: Intertropical Convergence Zone migrations and El Niño–Southern Oscillation variability. Geology 35, 21–24. https://doi.org/10.1130/G23125A.1

Russell, J.M., Verschuren, D., Eggermont, H., 2007. Spatial complexity of 'Little Ice Age' climate in East Africa: sedimentary records from two crater lake basins in western Uganda. The Holocene 17, 183–193. https://doi.org/10.1177/0959683607075832

Sachse, D., Radke, J., Gleixner, G., 2004. Hydrogen isotope ratios of recent lacustrine sedimentary n-alkanes record modern climate variability. Geochim. Cosmochim. Acta 68, 4877–4889. https://doi.org/10.1016/j.gca.2004.06.004

Sauer, P.E., Eglinton, T.I., Hayes, J.M., Schimmelmann, A., Sessions, A.L., 2001. Compound-specific D/H ratios of lipid biomarkers from sediments as a proxy for environmental and climatic conditions1. Geochim. Cosmochim. Acta 65, 213–222. https://doi.org/10.1016/S0016-7037(00)00520-2

Sessions, A.L., Burgoyne, T.W., Schimmelmann, A., Hayes, J.M., 1999. Fractionation of hydrogen isotopes in lipid biosynthesis. Org. Geochem. 30, 1193–1200. https://doi.org/10.1016/S0146-6380(99)00094-7

Sinkevičienė, Z., 2016. Caldesia Parnassifolia – not extinct in Lithuania. Bot. Lith. 22. https://doi.org/10.1515/botlit-2016-0004

Sinninghe Damsté, J.S., Hopmans, E.C., Pancost, R.D., Schouten, S., Geenevasen, J.A.J., 2000. Newly discovered non-isoprenoid glycerol dialkylglycerol tetraether lipids in sediments. Chem. Commun. 1683–1684. https://doi.org/10.1039/B004517I

Sinninghe Damsté, J.S., Ossebaar, J., Schouten, S., Verschuren, D., 2012. Distribution of tetraether lipids in the 25-ka sedimentary record of Lake Challa: extracting reliable TEX86 and MBT/CBT palaeotemperatures from an equatorial African lake. Quat. Sci. Rev. 50, 43–54. https://doi.org/10.1016/j.quascirev.2012.07.001

Stockmarr, J., 1971. Tablets with spores used in absolute pollen analysis. Pollen Spores 13, 615–621.

Swan, J.M.A., Gill, A.M., 1970. The origins, spread, and consolidation of a floating bog in Harvard pond, Petersham, Massachusetts. Ecology 51, 829–840. https://doi.org/10.2307/1933975

Swindles, G.T., Morris, P.J., Whitney, B., Galloway, J.M., Gałka, M., Gallego-Sala, A., Macumber, A.L., Mullan, D., Smith, M.W., Amesbury, M.J., Roland, T.P., Sanei, H., Patterson, R.T., Sanderson, N., Parry, L., Charman, D.J., Lopez, O., Valderamma, E., Watson, E.J., Ivanovic, R.F., Valdes, P.J., Turner, T.E., Lähteenoja, O., 2018. Ecosystem state shifts during long-term development of an Amazonian peatland. Glob. Change Biol. 24, 738–757. https://doi.org/10.1111/gcb.13950

Talling, J.F., Lemoalle, J., ORSTOM, 1998. Ecological dynamics of tropical inland waters, Cambridge University Press. ed. United Kingdom.

Thevenon, F., Williamson, D., Vincens, A., Taieb, M., Merdaci, O., Decobert, M., Buchet, G., 2003. A late-Holocene charcoal record from Lake Masoko, SW Tanzania: climatic and anthropologic implications. The Holocene 13, 785–792. https://doi.org/10.1191/0959683603hl665rr

Tierney, J.E., Russell, J.M., Huang, Y., Damsté, J.S.S., Hopmans, E.C., Cohen, A.S., 2008. Northern hemisphere controls on tropical southeast African climate during the past 60,000 Years. Science 322, 252–255. https://doi.org/10.1126/science.1160485

Tierney, J. E., Mayes, M.T., Meyer, N., Johnson, C., Swarzenski, P.W., Cohen, A.S., Russell, J.M., 2010a. Late-twentieth-century warming in Lake Tanganyika unprecedented since AD 500. Nat. Geosci. 3, 422–425. https://doi.org/10.1038/ngeo865

Tierney, J. E., Russell, J.M., Eggermont, H., Hopmans, E.C., Verschuren, D., Sinninghe Damsté, J.S., 2010b. Environmental controls on branched tetraether lipid distributions in tropical East African lake sediments. Geochim. Cosmochim. Acta 74, 4902–4918.

Tierney, J.E., Lewis, S.C., Cook, B.I., LeGrande, A.N., Schmidt, G.A., 2011. Model, proxy and isotopic perspectives on the East African Humid Period. Earth Planet. Sci. Lett. 307, 103–112. https://doi.org/10.1016/j.epsl.2011.04.038

Tierney, J.E., Smerdon, J.E., Anchukaitis, K.J., Seager, R., 2013. Multidecadal variability in East African hydroclimate controlled by the Indian Ocean. Nature 493, 389–392. https://doi.org/10.1038/nature11785

Trumbore, S., 2009. Radiocarbon and soil carbon dynamics. Annu. Rev. Earth Planet. Sci. 37, 47–66. https://doi.org/10.1146/annurev.earth.36.031207.124300
Tyson, P.D., Lindesay, J.A., 1992. The climate of the last 2000 years in southern Africa. The Holocene 2, 271–278. https://doi.org/10.1177/095968369200200310
van Geel, B., 1978. A palaeoecological study of Holocene peat bog sections in Germany and the Netherlands. Rev. Palaeobot. Palynol. 25, 1–120.
van Geel, B., Gelorini, V., Lyaruu, A., Aptroot, A., Rucina, S., Marchant, R., Damsté, J.S.S., Verschuren, D., 2011. Diversity and ecology of tropical African fungal spores from a 25,000-year palaeoenvironmental record in southeastern Kenya. Rev. Palaeobot. Palynol. 164, 174–190. https://doi.org/10.1016/j.revpalbo.2011.01.002
Vánky, K., 1998. New Australasian Ustilaginales. Mycotaxon 68, 327–344.
Velichkevich, F.Y., Zastawniak, E., 2006. Atlas of the Pleistocene vascular plant macrofossils of Central and Eastern Europe. Part 1-Pteridophytes and monocotyledons. W. Szafer Institute of Botany, Polish Academy of Sciences, Krakow, Poland.
Velichkevich, F.Y., Zastawniak, E., 2009. Atlas of the Pleistocene vascular plant macrofossils of Central and Eastern Europe. Part 2-Herbaceous dicotyledons. W. Szafer Institute of Botany, Polish Academy of Sciences, Krakow, Poland.
Verschuren, D., Laird, K.R., Cumming, B.F., 2000. Rainfall and drought in equatorial east Africa during the past 1,100 years. Nature 403, 410–414. https://doi.org/10.1038/35000179
Verschuren, D., 2003. Lake-based climate reconstruction in Africa: progress and challenges. Hydrobiologia 500, 315–330. https://doi.org/10.1023/A:1024686229778
Verschuren, D., Charman, D.J., 2008. Latitudinal Linkages in Late Holocene Moisture-Balance Variation, in: Battarbee, R.W., Binney, H.A. (Eds.), Natural Climate Variability and Global Warming. Wiley Blackwell, pp. 189–231. https://doi.org/10.1002/9781444300932.ch8
Vincens, A., Williamson, D., Thevenon, F., Taieb, M., Buchet, G., Decobert, M., Thouveny, N., 2003. Pollen-based vegetation changes in southern Tanzania during the last 4200 years: climate change and/or human impact. Palaeogeogr. Palaeoclimatol. Palaeoecol. 198, 321–334. https://doi.org/10.1016/S0031-0182(03)00473-5
Vincens, A., Lézine, A.-M., Buchet, G., Lewden, D., Le Thomas, A., 2007. African pollen database inventory of tree and shrub pollen types. Rev. Palaeobot. Palynol. 145, 135–141. https://doi.org/10.1016/j.revpalbo.2006.09.004
Wanner, H., Solomina, O., Grosjean, M., Ritz, S.P., Jetel, M., 2011. Structure and origin of Holocene cold events. Quat. Sci. Rev. 30, 3109–3123. https://doi.org/10.1016/j.quascirev.2011.07.010
Weijers, J.W.H., Schouten, S., Spaargaren, O.C., Sinninghe Damsté, J.S., 2006. Occurrence and distribution of tetraether membrane lipids in soils: Implications for the use of the TEX86 proxy and the BIT index. Org. Geochem. 37, 1680–1693. https://doi.org/10.1016/j.orggeochem.2006.07.018
Weijers, J.W.H., Schefuß, E., Schouten, S., Damsté, J.S.S., 2007a. Coupled thermal and hydrological evolution of tropical Africa over the Last Deglaciation. Science, New Series 315, 1701–1704.
Weijers, J.W.H., Schouten, S., van den Donker, J.C., Hopmans, E.C., Sinninghe Damsté, J.S., 2007b. Environmental controls on bacterial tetraether membrane lipid distribution in soils. Geochim. Cosmochim. Acta 71, 703–713. https://doi.org/10.1016/j.gca.2006.10.003
Weijers, J.W.H., Panoto, E., van Bleijswijk, J., Schouten, S., Rijpstra, W.I.C., Balk, M., Stams, A.J.M., Damsté, J.S.S., 2009. Constraints on the biological source(s) of the orphan branched tetraether membrane lipids. Geomicrobiol. J. 26, 402–414. https://doi.org/10.1080/01490450902937293

White, F., 1983. Vegetation of Africa - a descriptive memoir to accompany the Unesco/AETFAT/UNSO vegetation map of Africa.

Woodborne, S., Hall, G., Robertson, I., Patrut, A., Rouault, M., Loader, N.J., Hofmeyr, M., 2015. A 1000-year carbon isotope rainfall proxy record from south African Baobab trees (Adansonia digitata L.). PLOS ONE 10, e0124202. https://doi.org/10.1371/journal.pone.0124202

Highlights

- 4000-year continuous peat record of the Late Holocene in East Africa (SW Tanzania).
- Multi proxy approach evidences major ecological changes at ca. 2500 yr cal. BP.
- Detailed temperature and hydrology records highlight several cold events.
- More recent climate conditions seem connected to South African climate variability.

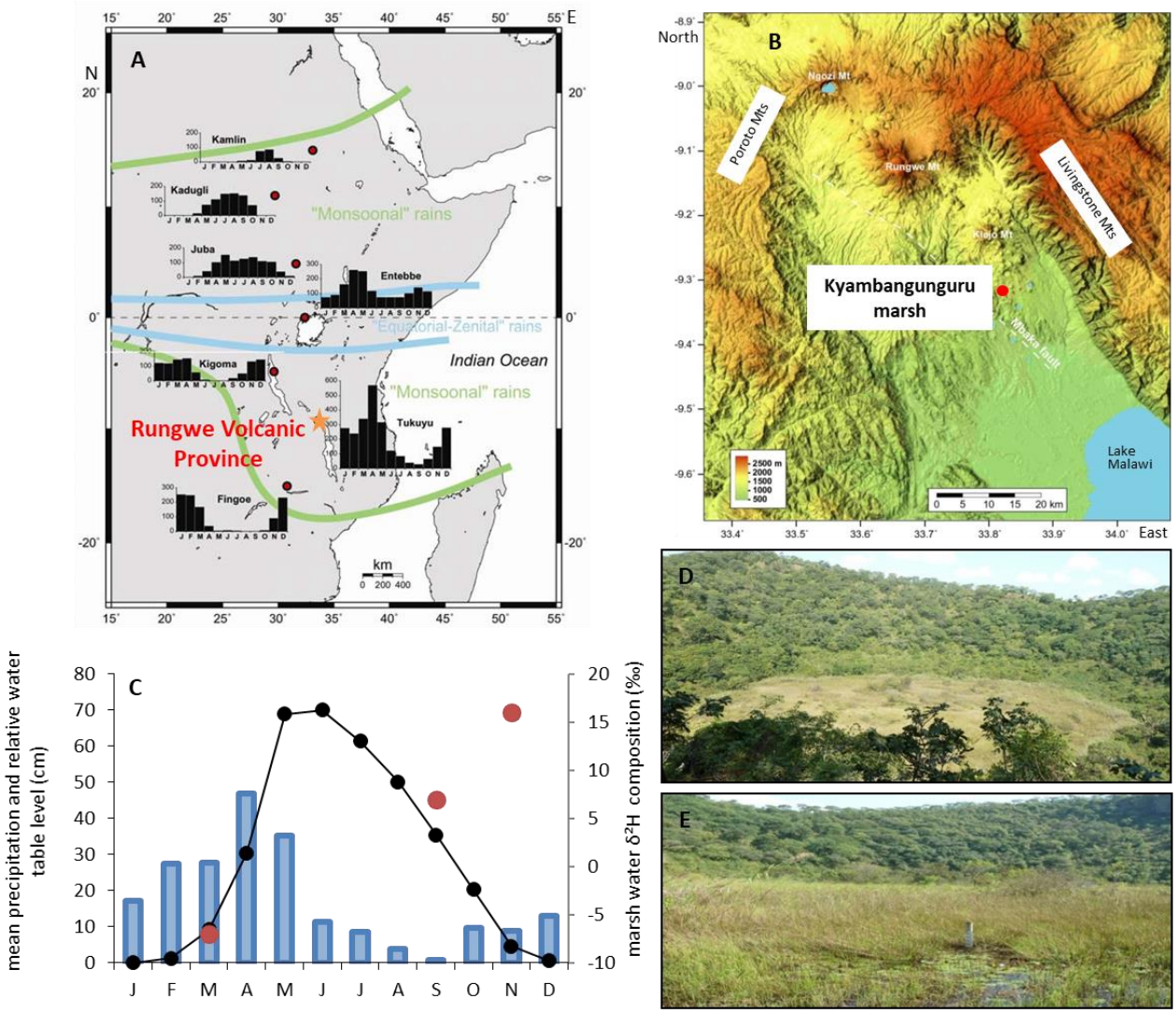
A
Kamlin
Kadugli
Juba
Entebbe
Kigoma
Tukuyu
Fingoe
"Monsoonal" rains
"Equatorial-Zenital" rains
"Monsoonal" rains
Indian Ocean
Rungwe Volcanic Province
km
B
North
East
Ngozi Mt
Rungwe Mt
Kiejo Mt
Poroto Mts
Livingstone Mts
Kyambangunguru marsh
L. Malawi fault
Lake Malawi
C
mean precipitation and relative water table level (cm)
marsh water δ2H composition (‰)
J F M A M J J A S O N D
D
E

Figure 1.

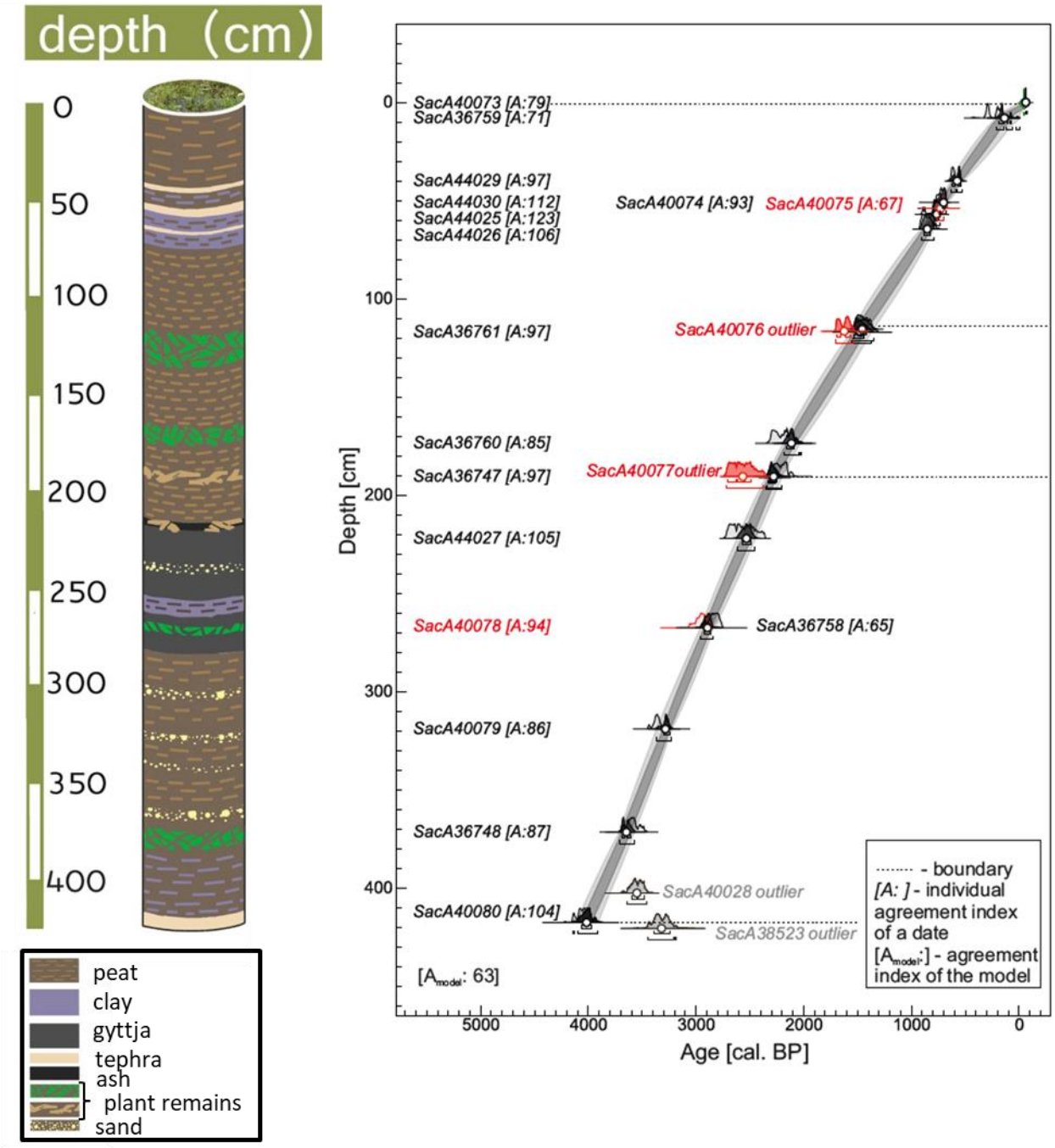
depth (cm)
0
50
100
150
200
250
300
350
400
peat
clay
gyttja
tephra
ash
plant remains
sand
Depth [cm]
Age [cal. BP]
SacA40073 [A:79]
SacA36759 [A:71]
SacA44029 [A:97]
SacA44030 [A:112]
SacA44025 [A:123]
SacA44026 [A:106]
SacA40074 [A:93]
SacA40075 [A:67]
SacA36761 [A:97]
SacA40076 outlier
SacA36760 [A:85]
SacA36747 [A:97]
SacA40077outlier
SacA44027 [A:105]
SacA40078 [A:94]
SacA36758 [A:65]
SacA40079 [A:86]
SacA36748 [A:87]
SacA40028 outlier
SacA40080 [A:104]
SacA38523 outlier
[A_model: 63]
..... - boundary
[A:] - individual agreement index of a date
[A_model:] - agreement index of the model

Figure 2.

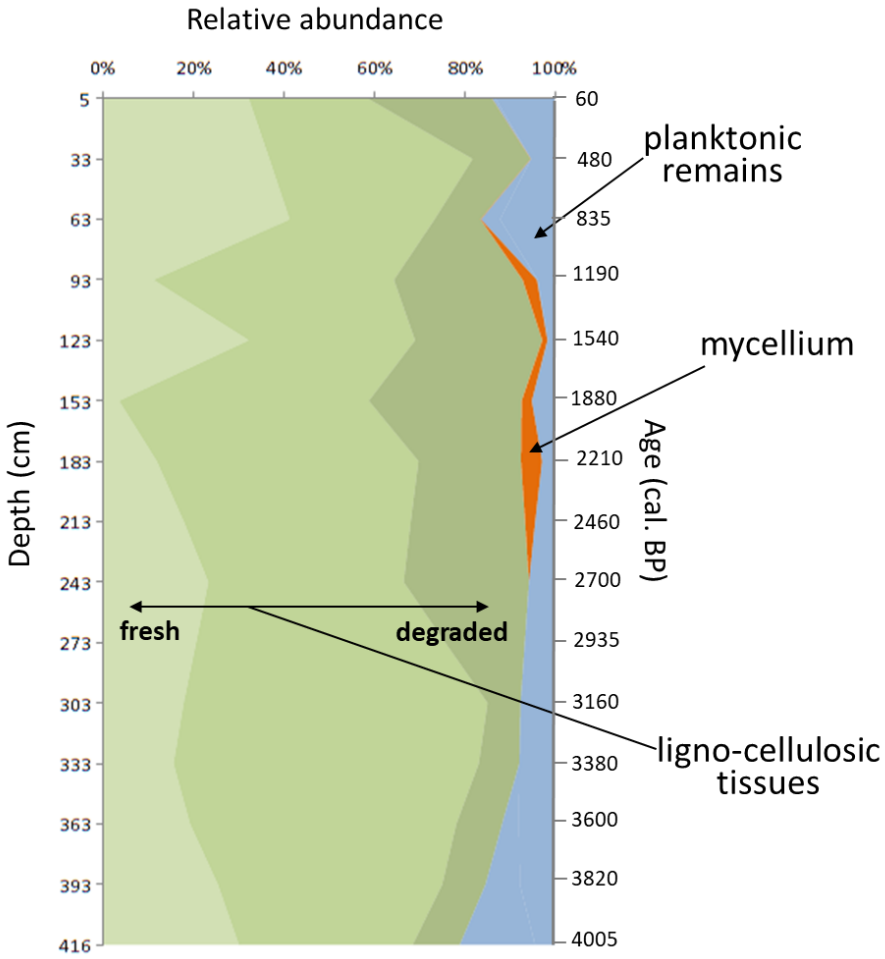
Relative abundance
0%
20%
40%
60%
80%
100%
Depth (cm)
5
33
63
93
123
153
183
213
243
273
303
333
363
393
416
Age (cal. BP)
60
480
835
1190
1540
1880
2210
2460
2700
2935
3160
3380
3600
3820
4005
planktonic remains
mycellium
fresh
degraded
ligno-cellulosic tissues

Figure 3.

Figure 4.

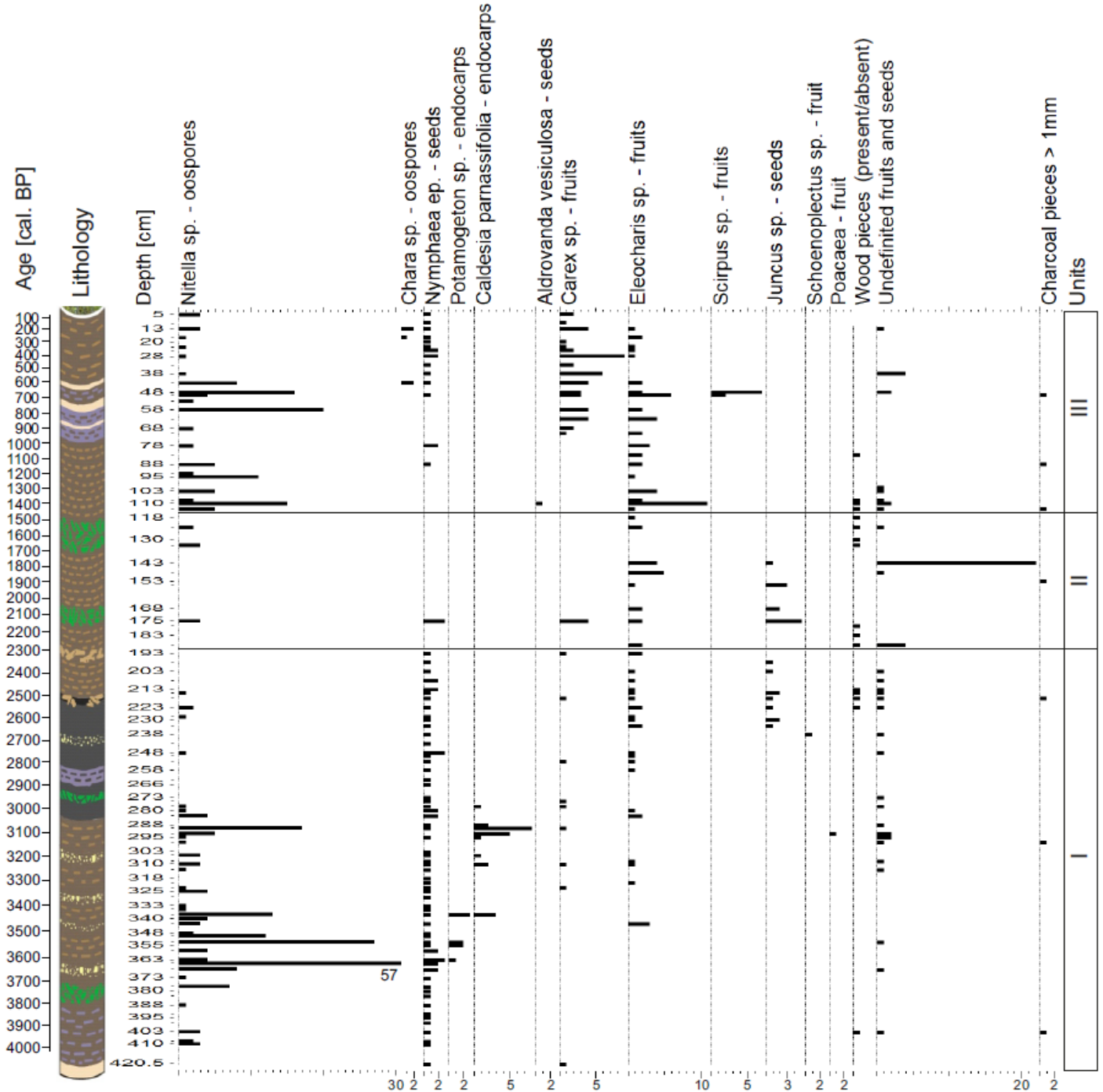
Age [cal. BP]
Lithology
Depth [cm]
Nitella sp. - oospores
Chara sp. - oospores
Nymphaea ep. - seeds
Potamogeton sp. - endocarps
Caldesia parnassifolia - endocarps
Aldrovanda vesiculosa - seeds
Carex sp. - fruits
Eleocharis sp. - fruits
Scirpus sp. - fruits
Juncus sp. - seeds
Schoenoplectus sp. - fruit
Poacaea - fruit
Wood pieces (present/absent)
Undefinited fruits and seeds
Charcoal pieces > 1mm
Units
I
II
III
57

Figure 5.

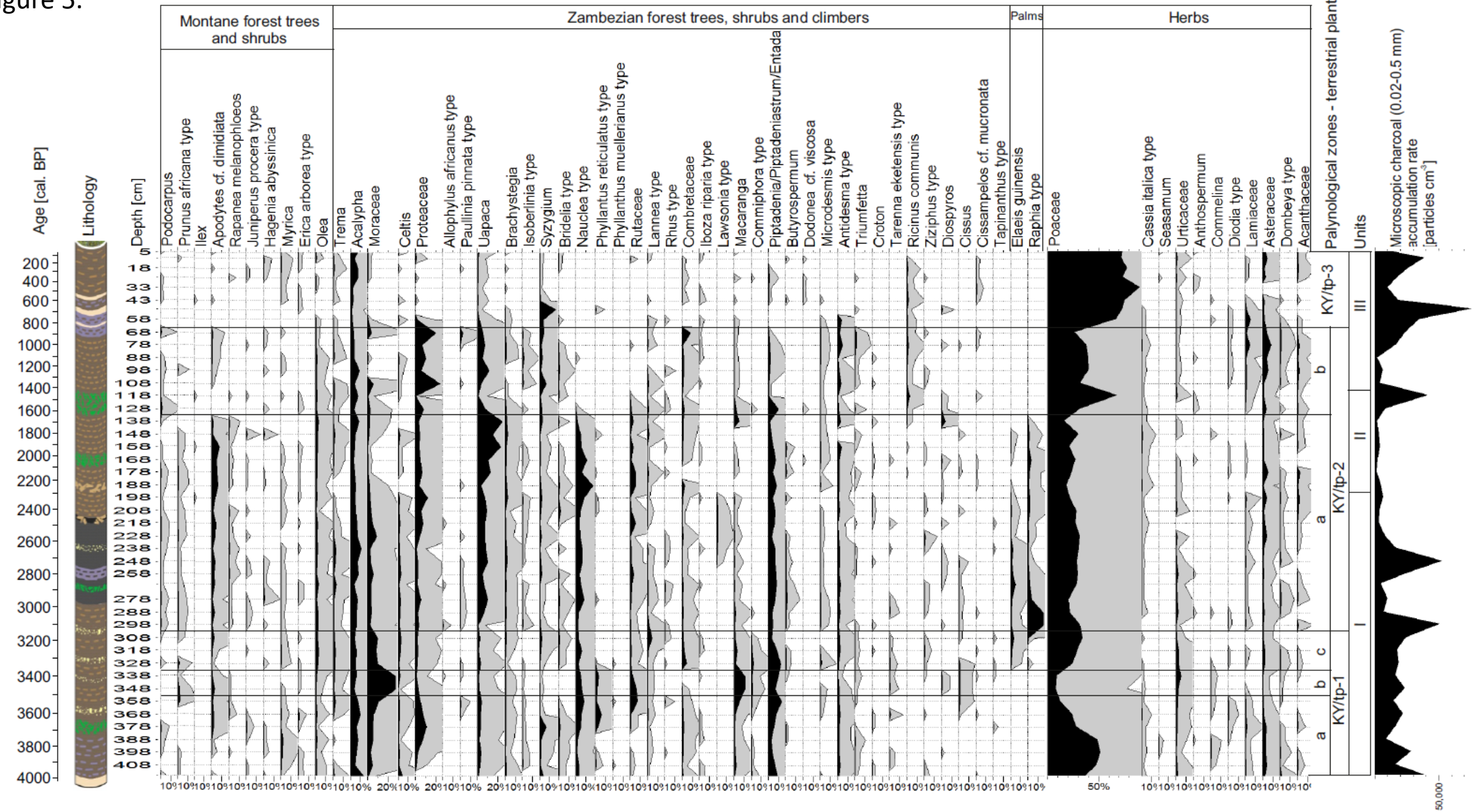
Montane forest trees and shrubs
Zambezian forest trees, shrubs and climbers
Palms
Herbs
Podocarpus
Prunus africana type
Ilex
Apodytes cf. dimidiata
Rapanea melanophloeos
Juniperus procera type
Hagenia abyssinica
Myrica
Erica arborea type
Olea
Trema
Acalypha
Moraceae
Celtis
Proteaceae
Allophylus africanus type
Paullinia pinnata type
Uapaca
Brachystegia
Isoberlinia type
Syzygium
Bridelia type
Nauclea type
Phyllantus reticulatus type
Phyllanthus muellerianus type
Rutaceae
Lannea type
Rhus type
Combretaceae
Iboza riparia type
Lawsonia type
Macaranga
Commiphora type
Piptadenia/Piptadeniastrum/Entada
Butyrospermum
Dodonea cf. viscosa
Microdesmis type
Antidesma type
Triumfetta
Croton
Tarenna eketensis type
Ricinus communis
Ziziphus type
Diospyros
Cissus
Cissampelos cf. mucronata
Tapinanthus type
Elaeis guinensis
Raphia type
Poaceae
Cassia italica type
Seasamum
Urticaceae
Anthospermum
Commelina
Diodia type
Lamiaceae
Asteraceae
Dombeya type
Acanthaceae
Age [cal. BP]
Lithology
Depth [cm]
Palynological zones - terrestrial plants
Units
KY/tp-3
KY/tp-2
KY/tp-1
Microscopic charcoal (0.02-0.5 mm) accumulation rate [particles cm-3]

Figure 6.

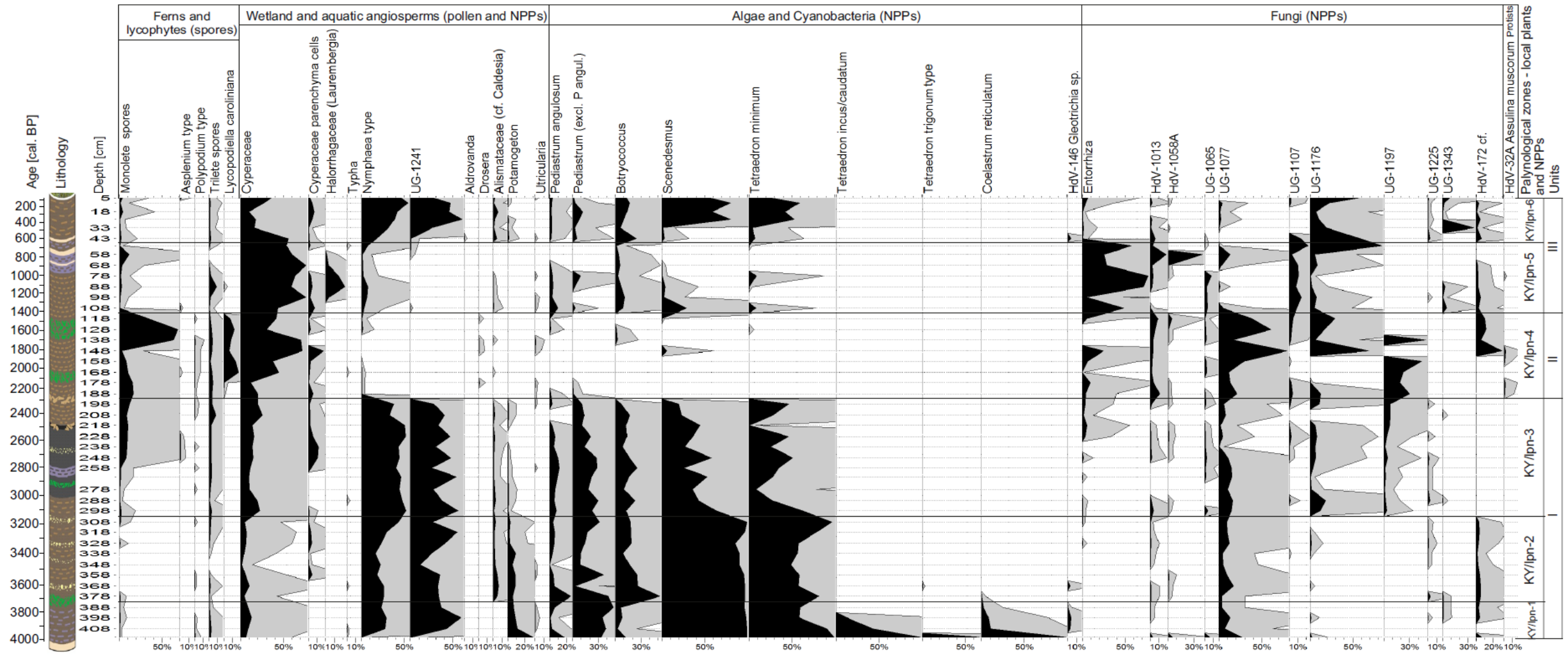
Ferns and lycophytes (spores)
Wetland and aquatic angiosperms (pollen and NPPs)
Algae and Cyanobacteria (NPPs)
Fungi (NPPs)
Age [cal. BP]
Lithology
Depth [cm]
Monolete spores
Asplenium type
Polypodium type
Trilete spores
Lycopodiella caroliniana
Cyperaceae
Cyperaceae parenchyma cells
Halorrhagaceae (Laurembergia)
Typha
Nymphaea type
UG-1241
Aldrovanda
Drosera
Alismataceae (cf. Caldesia)
Potamogeton
Utricularia
Pediastrum angulosum
Pediastrum (excl. P angul.)
Botryococcus
Scenedesmus
Tetraedron minimum
Tetraedron incus/caudatum
Tetraedron trigonum type
Coelastrum reticulatum
HdV-146 Gleotrichia sp.
Entorrhiza
HdV-1013
HdV-1058A
UG-1065
UG-1077
UG-1107
UG-1176
UG-1197
UG-1225
UG-1343
HdV-172 cf.
HdV-32A Assulina muscorum
Protists
Palynological zones - local plants and NPPs
Units
KY/lpn-6
KY/lpn-5
KY/lpn-4
KY/lpn-3
KY/lpn-2
KY/lpn-1
III
II
I

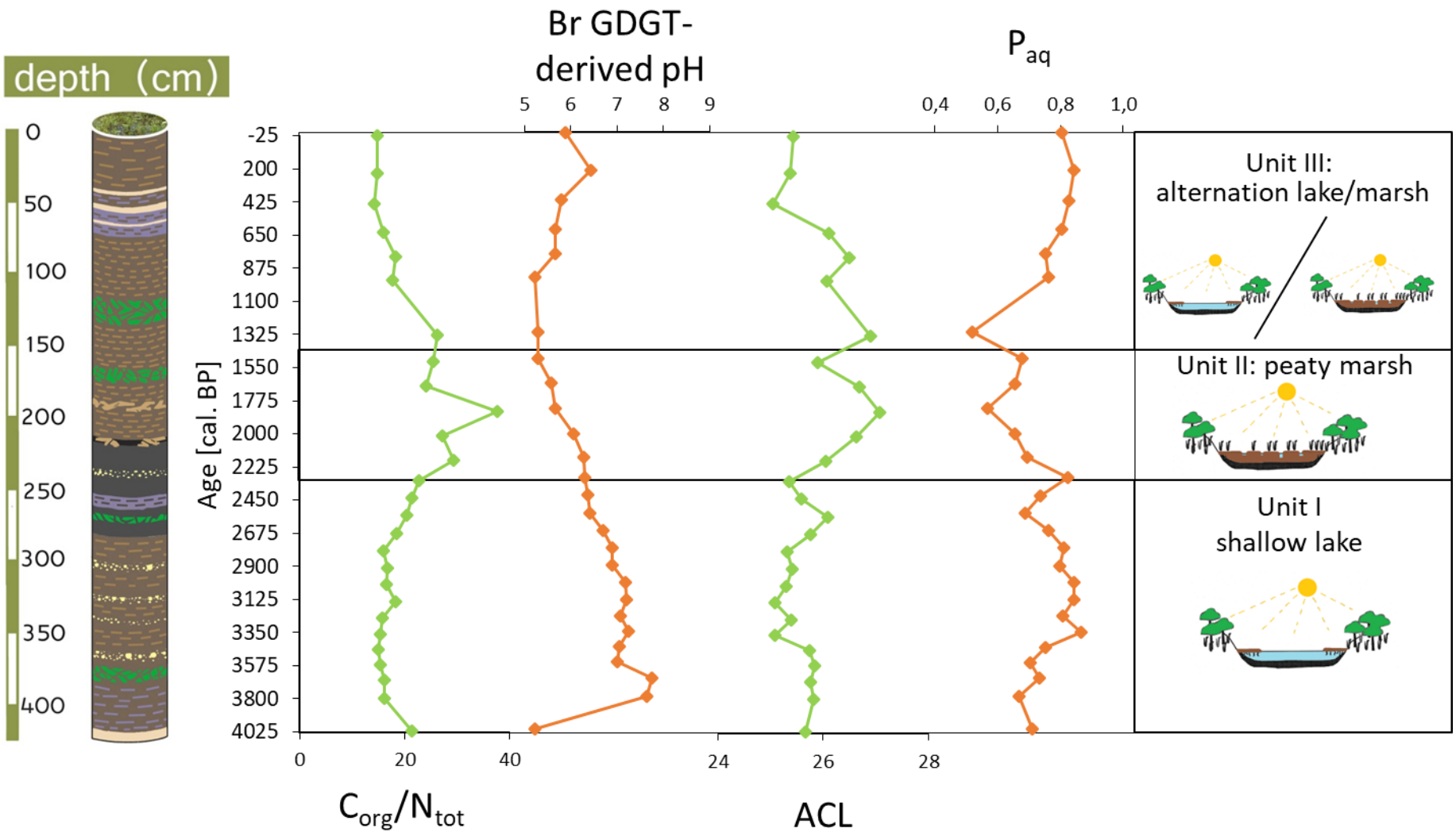
depth (cm)
0
50
100
150
200
250
300
350
400
Br GDGT-derived pH
5
6
7
8
9
P_{aq}
0,4
0,6
0,8
1,0
Age [cal. BP]
-25
200
425
650
875
1100
1325
1550
1775
2000
2225
2450
2675
2900
3125
3350
3575
3800
4025
0
20
40
24
26
28
C_{org}/N_{tot}
ACL
Unit III: alternation lake/marsh
Unit II: peaty marsh
Unit I shallow lake

Figure 7.

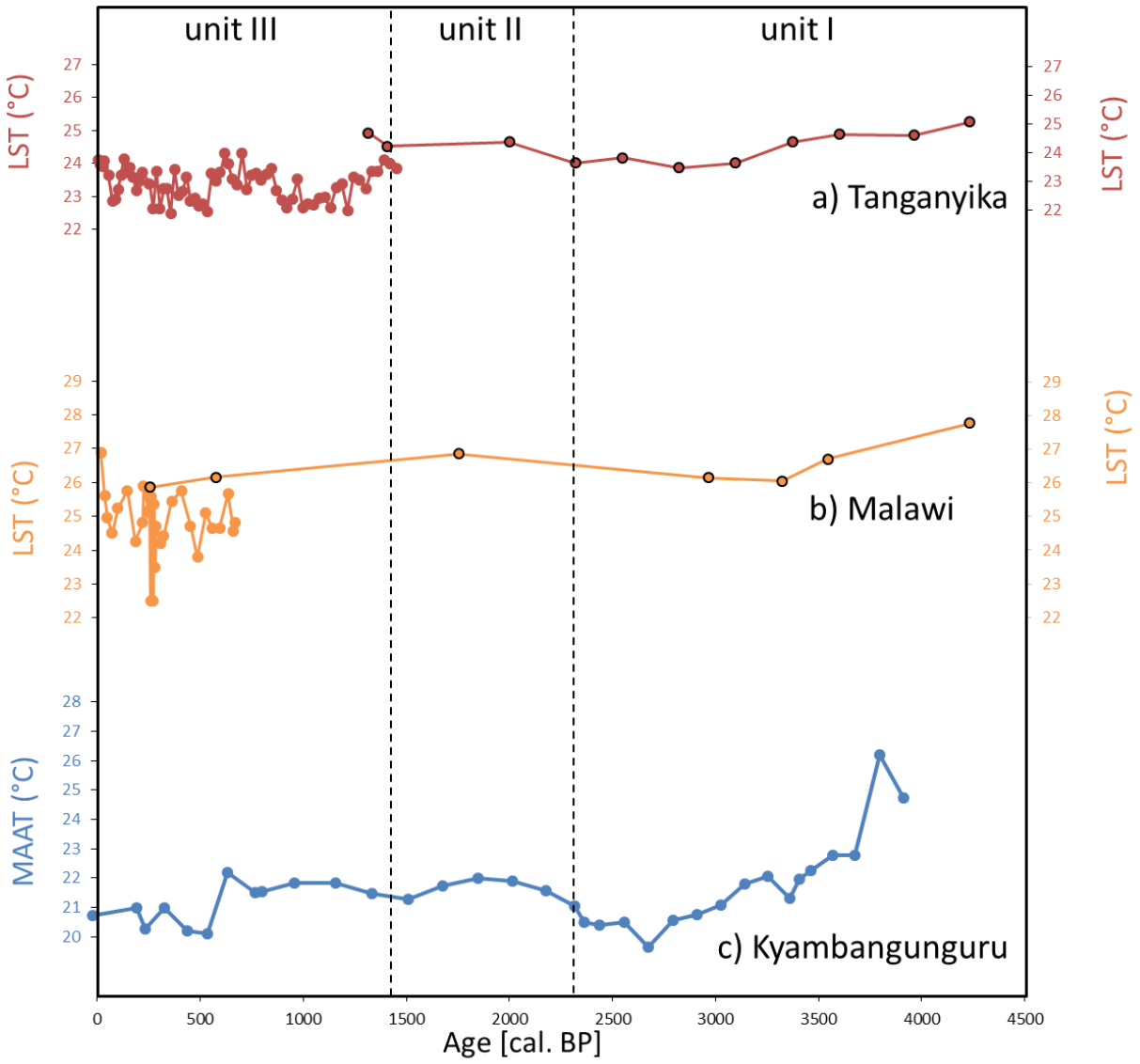
unit III
unit II
unit I
LST (°C)
a) Tanganyika
b) Malawi
MAAT (°C)
c) Kyambangunguru
Age [cal. BP]
0
500
1000
1500
2000
2500
3000
3500
4000
4500

Figure 8.

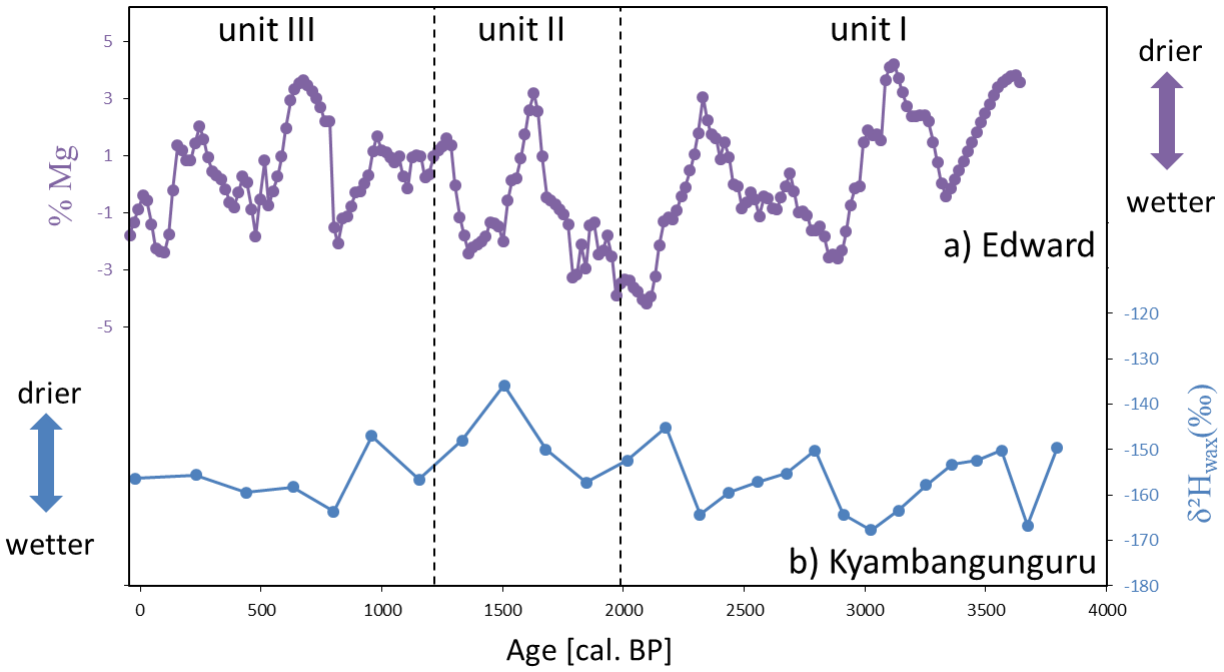
unit III
unit II
unit I
drier
wetter
% Mg
a) Edward
b) Kyambangunguru
drier
wetter
δ^2H_{wax}(‰)
Age [cal. BP]

Figure 9.

Table 1.

Depth (cm)	AMS ^{14}C measure ref	Type of material	Carbon mass (mg)	^{14}C activity (pMC)	Measured ^{14}C age (cal. BP)	Calibrated age range [cal. BP; 95.4% (2 σ) range]	Modelled age ± σ error (cal. BP)	$\delta^{13}C$ (‰)
0.5	SacA40073	TOM	1.82	112.21 ± 0.33	Post 1950	-8–-8 (3.3 %) -43–-46 (88.4 %) -47–-47 (3.7 %)	-45±5	-29.5
8.0	SacA36759	TOM	0.75	96.86 ± 0.43	255 ± 35	435–408 (1.9 %) 325–254 (39.4 %) 225–143 (54.2 %)	135±50	-24.5
40.0	SacA44029	TOM	0.75	92.48 ± 0.24	630 ± 30	646–588 (58.7 %) 574–535 (36.7 %)	574±28	-23.8
51.0	SacA44030	TOM	0.75	89.99 ± 0.27	845 ± 30	763–673	701±15	-22.9
54.0	SacA40074	TOM	0.55	89.53 ± 0.29	890 ± 30	800–682	730±14	-28.0
54.0	SacA40075	Wood	0.91	90.27 ± 0.36	825 ± 30	742–666	729±14	-25.2
57.0	SacA44025	TOM	0.75	89.20 ± 0.23	920 ± 30	905–861 (14.1 %) 842–829 (1.3 %) 820–724 (80 %)	765±17	-21.4
64.0	SacA44026	TOM	0.75	88.55 ± 0.24	975 ± 30	921–774	852±30	-20.2
116.5	SacA36761	TOM	0.50	82.03 ± 0.48	1590 ± 45	1538–1348 (94.6 %) 1331–1324 (0.8 %)	1472±47	-25.5
116.5	SacA40076	Wood	1.37	80.47 ± 0.28	1745 ± 30	1702–1639 (39.3 %) 1633–1542 (56.1 %)	Not applied	-28.2
173.5	SacA36760	TOM	0.75	75.90 ± 0.38	2215 ± 40	2318–2059	2113±37	-20.1
190.5	SacA36747	TOM	0.75	75.68 ± 0.31	2240 ± 35	2328–2146 (90.1 %) 2131–2103 (5.3 %)	2278±34	-25.0
190.5	SacA40077	Wood	1.30	73.12 ± 0.26	2515 ± 30	2719–2379	Not applied	-27.5
222.0	SacA44027	TOM	0.75	73.18 ± 0.22	2510 ± 30	2715–2379	2531±42	-26.8
267.5	SacA36758	TOM	0.75	70.72 ± 0.37	2785 ± 40	2945–2759	2892±30	-27.9

267.5	SacA40078	Wood	1.40	69.87 ± 0.25	2880 ± 30	3062–2857	2893±30	-27.9
319.0	SacA40079	TOM	1.11	67.41 ± 0.25	3170 ± 30	3445–3423 (4.8%) 3411–3236 (90.6 %)	3283±34	-28.6
371.5	SacA36748	TOM	0.75	65.50 ± 0.29	3395 ± 35	3692–3657 (10.4 %) 3651–3478 (85 %)	3646±37	-28.2
402.0	SacA44028	TOM	0.75	65.76 ± 0.21	3365 ± 30	3639–3456	Not applied	-26.4
417.5	SacA40080	TOM Tephra	1.04	62.75 ± 0.24	3745 ± 30	4151–3960 (91.1 %) 3950–3926 (4.3 %)	4015±47	-20.0
420.5	SacA38523	TOM Tephra	0.30	67.47 ± 0.42	3160 ± 50	3450–3206 (93.8 %) 3197–3182 (1.6 %)	Not applied	-23.6